Int J Earth Sci (Geol Rundsch) (2016) 105:819–847
DOI 10.1007/s00531-015-1210-2

ORIGINAL PAPER

The Late Cretaceous igneous rocks of Romania (Apuseni Mountains and Banat): the possible role of amphibole versus plagioclase deep fractionation in two different crustal terranes

Jacqueline Vander Auwera[1] · Tudor Berza[2] · Julie Gesels[1] · Alain Dupont[1,2,3]

Received: 22 March 2015 / Accepted: 2 June 2015 / Published online: 27 June 2015

Abstract We provide new whole-rock major and trace elements as well as $^{87}Sr/^{86}Sr$ and $^{143}Nd/^{144}Nd$ isotopic data of a suite of samples collected in the Late Cretaceous volcanic and plutonic bodies of the Apuseni Mts. (Romania) that belong to the Banatitic Magmatic and Metallogenic Belt, also called the Apuseni–Banat–Timok–Srednogorie belt. The samples define a medium- to high-K calc-alkaline differentiation trend that can be predicted by a three-step fractional crystallization process which probably took place in upper crustal magma chambers. Published experimental data indicate that the parent magma (Mg# = 0.47) of the Apuseni Mts. trend could have been produced by the lower crustal differentiation of a primary (in equilibrium with a mantle source) magma. The Late Cretaceous magmatic rocks of the Apuseni Mts. and Banat display overlapping major and trace element trends except that Sr is slightly lower and Ga is higher in the Apuseni Mts. parent magma. This difference can be accounted for by fractionating plagioclase-bearing (Apuseni Mts.) or amphibole-bearing (Banat) cumulates during the lower crustal differentiation of the primary magma to the composition of the parent magma of both trends. This, together with results obtained on the Late Cretaceous igneous rocks from the Timok area in Eastern Serbia, further suggests variation of the water content of the primary magma along and across the belt. The Apuseni Mts. versus the Banat samples display different isotopic compositions that likely resulted from the assimilation of two distinct crustal contaminants, in agreement with their emplacement in two separate mega-units of Alpine Europe.

Keywords Fractional crystallization · Sr and Nd isotopes · Amphibole · Water content

Introduction

The Apuseni Mts. are part of the 1500-km-long Late Cretaceous Banatitic or Apuseni–Banat–Timok–Srednogorie Magmatic and Metallogenic belt that stretches across southeastern Europe from Romania, through Serbia and Bulgaria (Berza et al. 1998; Popov et al. 2002). Late Cretaceous magmatic rocks are also known from drillings in the Tatra Mts. of Slovakia (Kohut et al. 2013) and in the north-eastern part of the Pannonian Basin (NE Hungary–NW Romania) (Berza and Ilinca 2014). In outcrop, a NE–SW orientation in the Apuseni Mts. and the western end of South Carpathians (Banat) turns to N–S in Eastern Serbia (Timok and Ridanj-Krepolijn) and finally to E–W in Bulgaria (Srednogorie) (Fig. 1). This present-day orientation is due to a 80° clockwise rotation of the Tisza and Dacia units during the Cenozoic (Panaiotu 1998), turning the Tatra–Apuseni–Banat part from an original E–W orientation to a N–S one. The Banatitic belt contains abundant ore deposits ranging from Cu–Au–Ag epithermal deposits to Fe–Pb–Zn–Mo skarn and Cu–Mo–Au porphyry (Berza and Ilinca 2014). Precise Re–Os geochronological data acquired on molybdenite from

Electronic supplementary material The online version of this article (doi:10.1007/s00531-015-1210-2) contains supplementary material, which is available to authorized users.

✉ Jacqueline Vander Auwera
jvdauwera@ulg.ac.be

[1] Department of Geology, University of Liege, 4000 Sart Tilman, Belgium

[2] Institutul Geologic al României, 1 Caransebeș street, 78344 Bucharest, Romania

[3] Laboratoire de Géologie, Université Blaise Pascal, 5 Rue Kessler, 63038 Clermont-Ferrand, France

Fig. 1 Schematic geological map of Roumania displaying the location of the studied intrusions

these ore deposits (Zimmerman et al. 2008; Kohut et al. 2013) and U–Pb LA-ICPMS ages obtained on the magmatic zircon (Nicolescu et al. 1999; Von Quadt et al. 2005; Georgiev et al. 2012; Kohut et al. 2013; Kolb et al. 2013) indicate the following bracketing ages for intrusion and/or molybdenite crystallization: Tatra (U–Pb: 81 Ma—Re–Os: 81 Ma), Apuseni (Re–Os: 79–80 Ma), Banat (Re–Os: 72–83 Ma—U–Pb: 76–79 Ma), Ridanj-Krepolijn (U–Pb: 71–76 Ma), Timok (Re–Os: 81–88 Ma—U–Pb: 79–89 Ma) and Srednogorie (Re–Os: 87–92 Ma—U–Pb: 78–92 Ma).

The geodynamic setting of the Late Cretaceous magmatic rocks, named "banatites" (Von Cotta 1864), was mostly considered as subduction-related because of their calc-alkaline composition, their enrichment in LILE and depletion in Nb–Ta and the presence of a major oceanic remnant in the Carpathian–Balkan orogen, namely the Eastern Vardar Ocean (a branch of the Tethys Ocean) that is supposed to have subducted northward under the European margin during the Jurassic to Lower Cretaceous and to which the ophiolites of the Mureş zone (or

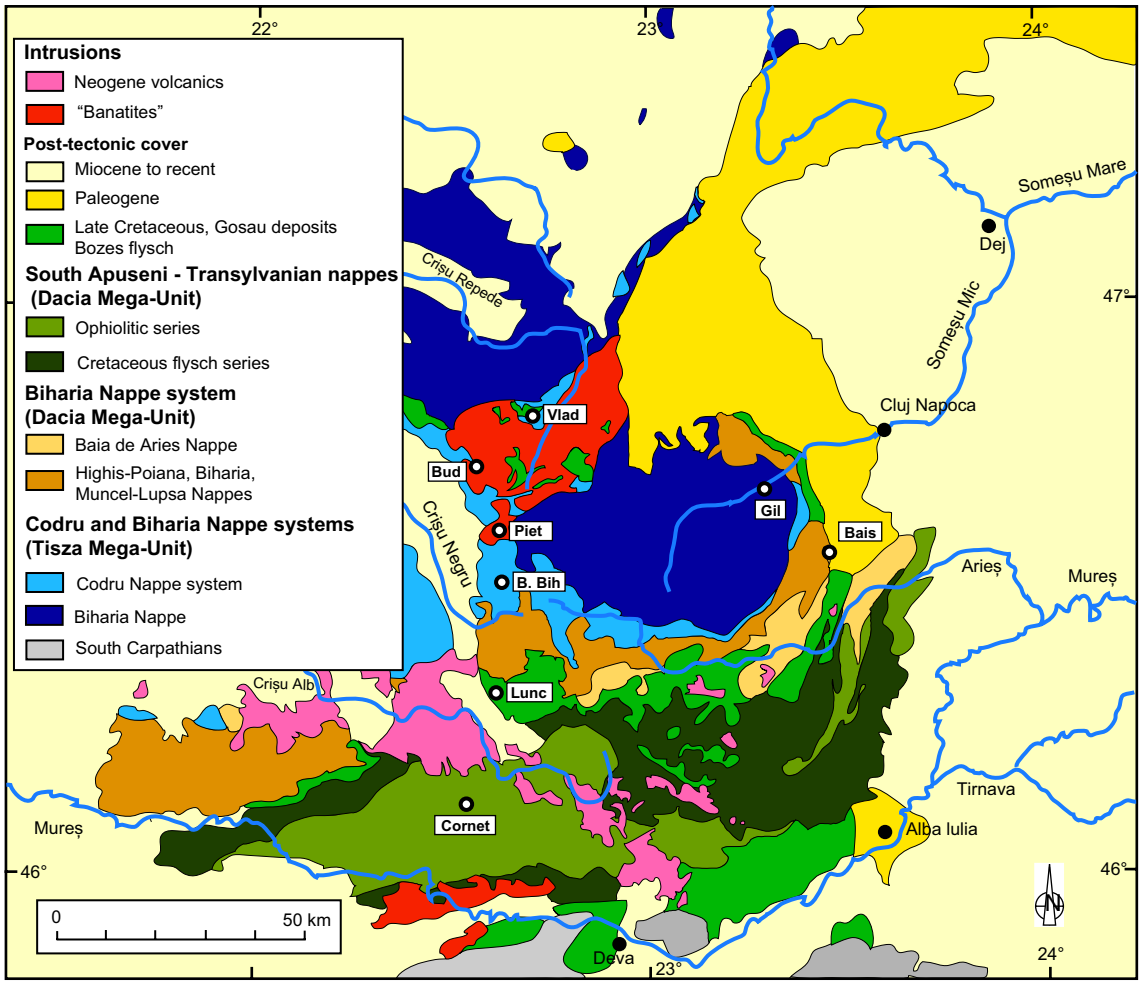

Fig. 2 Schematic tectonic map of the Apuseni Mts. (after Kounov and Schmid 2013) showing the location of the Late Cretaceous magmatic bodies that are sampled in this study. *Vlad* Vlădeasa, *Bud* Budureasa, *Piet* Pietroasa, *B. Bih.* Băiţa Bihor, *Lunc* Luncsoara, *Bais* Băişoara, *Gil* Gilau

Transylvanides) are linked (Schmid et al. 2008) (Figs. 1, 2). However, their precise geodynamic setting is still debated (Berza and Ilinca 2014). Based on their occurrence in Upper Cretaceous Gosau-type sedimentary basins that post-date the Mid-Cretaceous nappe empilement, several authors consider that they were emplaced in an extensional regime caused by orogenic collapse (Giuşcă et al. 1969; Antonijević et al. 1974; Popov 1981; Berza et al. 1998; Popov et al. 2002; Georgiev et al. 2012) or slab rollback (e.g. Von Quadt et al. 2005; Zimmerman et al. 2008; Schuller et al. 2009; Kolb et al. 2013). Neubauer (2002) interpreted this magmatism either as Andean-type or post-collisional and resulting from slab break-off or continuous subduction. Quantification of the magmatic processes that produced these igneous rocks provides independent constraints that help deciphering their origin. Detailed petrological informations are now available for the Banat region of southern Romania (Dupont et al. 2002) as well as for the Timok and Ridanj-Krepolijn regions of Eastern Serbia (Kolb et al. 2013). In this study, we analyse the petrogenesis of Late Cretaceous magmatic rocks outcropping in the Apuseni Mts., using new major and trace element, and isotopic data (Sr, Nd) on a series of samples collected in this region. We discuss their differentiation processes, their possible mantle-derived parent magmas and plausible contaminants. These data, together with the recent recognition of adakite-like magmas in the Timok and Ridanj-Krepolijn regions of NE Serbia (Kolb et al. 2013), enable us to propose that the H_2O content of the mantle-derived magmas from which the Late Cretaceous magmas differentiated varied along the belt.

Geological setting

The Apuseni Mts. are part of the Carpathians of Romania and represent a huge basement outcrop between the Neogene Transylvanian and Pannonian Basins (Fig. 2). The

southern Apuseni Mts. essentially comprise ophiolites of Jurassic age (the Metaliferi Mts.) that represent a branch of Neotethys, known as the Mureş zone (Savu 1996) or Transylvanian nappes (Rădulescu and Săndulescu 1973). The northern Apuseni Mts. are made of a sequence of several nappe systems that was formed during the continental collision (e.g. Schmid et al. 2008; Kounov and Schmid 2013). Each nappe system comprises crystalline basement rocks that deformed and metamorphosed during the Variscan orogeny. These basement rocks were intruded by Variscan granitoids and later covered by a sequence of sedimentary rocks of Permian to Late Cretaceous age (e.g. Pană et al. 2002; Balintoni et al. 2009). The boundary between the Tisza and Dacia Mega-Units, the South Transylvanian fault, passes through the Apuseni Mts. The two southern nappe sequences are attributed to the Dacia Mega-Unit, whereas the northern ones are interpreted as belonging to the Tisza Mega-Unit. However, the exact limit between the two Mega-Units is still debated (Csontos and Vörös 2004; Schmid et al. 2008). During the Late Cretaceous post-orogenic collapse of the orogen, sedimentary Gosau-type basins were formed because of extensional processes (Willingshofer et al. 1999; Schuller 2004; Schuller et al. 2009). The Late Cretaceous magmatic rocks are observed as volcanics in the Gosau-type basins and as shallow intrusions and volcanic bodies that are spread all over the Apuseni Mts. mostly as small occurrences (e.g. Budureasa, Pietroasa, Băişoara, Băiţa Bihor) except the Vlădeasa volcano-plutonic complex, situated in the northern part, that covers an area of more than 600 km^2 (Istrate 1978; Stefan 1980; Stefan et al. 1982, 1992) (Fig. 2).

Detailed mapping of the Late Cretaceous magmatic rocks outcropping in the Apuseni Mts. was performed by Istrate (1978), Stefan (1980), Stefan et al. (1982, 1992) and Ionescu (1997). These authors recognized volcanic and plutonic facies that range in composition from andesites/quartz diorites to dacites and rhyolites/granites. Istrate (1978), Stefan (1980) and Stefan et al. (1982) have also described dark fine-grained dykes, referred to as lamprophyres, that are up to 1 m of thickness and intrude the Senonian deposits as well as the volcanic and eruptive Late Cretaceous igneous rocks. Field evidence indicates that Vlădeasa volcanic rocks cover sedimentary rocks of Upper Coniacian–Lower Maastrichtian age and are themselves included in conglomerates of Palaeocene–Ypresian age (Stefan et al. 1992). K–Ar ages of 61 ± 3 and 61.5 ± 5 Ma were obtained on the Vlădeasa rhyolite by Bleahu et al. (1984). These ages are similar to those obtained on pre-Mesozoic Bihor crystalline schists, pointing to the presence of a significant thermal aureole of Banatitic plutons, also expressed by aeromagnetic and gravimetric anomalies (Andrei et al. 1989). Important ore bodies are associated with the granodiorites and granites as, for example, the Mo–Cu skarn of Băiţa Bihor dated between 80.63 ± 0.3 and 78.69 ± 0.4 Ma (Re/Os on molybdenite) (Zimmerman et al. 2008). This is currently the most accurate isotopic age obtained on Late Cretaceous igneous rocks from the Apuseni Mts., but ongoing research from ETH Zürich will soon present U–Pb zircon ages.

Sampling and methods

Because of the abundant vegetation in the region of the Apuseni Mts., the number and extension of the outcrops are rather limited. This hampers detailed observations of the relationships between different facies within one intrusion and also of the relationships of one particular intrusion with its surroundings rocks. Sixty-one samples were collected in a series of intrusions [Cornet (2), Luncsoara (4), Băiţa Bihor (1), Pietroasa (15), Budureasa (8), Vlădeasa (21), Băişoara (9), Gilau (1)] and care was taken in the field to sample fresh rocks (Table 1; Fig. 2). This is witnessed by the absent to weak alteration observed in thin sections, except in a few samples that were not considered for geochemistry, and by the low loss on ignition (LOI) (0.78 to 3.56 wt% with an average of 1.7 wt%) (Table 2). Moreover, mobile elements such as Ba, Sr, Pb and Mn are not correlated with the LOI.

A selection of thirty-two samples were crushed with a hammer and pulverized in an agate planetary mill (Gesels 2003). Fused glass discs prepared with lithium tetra- and meta-borate and 0.35 g of rock powder previously dried at 1000 °C for 2 h were used to measure major elements by X-ray fluorescence (ARL 9400 XP wavelength-dispersive (WD)-XRF spectrometer, University of Liège). Some trace elements (Ba, V, Cr, Ni, Cu, Zn) were also measured by X-ray fluorescence on pressed powdered pellets. The rest of the trace elements were determined by inductively coupled plasma mass spectrometry (VG Elemental PQ2+, University of Liège) following the method described by Vander Auwera et al. (1998) (Table 2). Accuracy is 1–3 % for major elements and ≤5 % for trace elements (Table 2).

Electron microprobe analyses of feldspars, amphibole, clinopyroxene and biotite were performed on a selection of polished thin sections from the different intrusions (samples R6 from Cornet, R10 from Luncsoara, R23 from Pietroasa, R30 from Budureasa, R43 from Vlădeasa, and R63 and R64 from Băişoara) with the Cameca SX50 hosted at the Ruhr-Universiteit Bochum (Supplementary Material S1a to S1e). An accelerating voltage of 15 kV was used, and elements were counted for 10 s at a beam current of 10 nA. Silicate and oxide standards were used, and X-ray intensities were reduced with the Cameca PAP correction program.

Table 1 Sample name and location

Intrusion	Sample #	Rock type	Long.(deg min sec)	Lat.(deg min sec)
Cornet	R04	Dacite	22 32 15	46 06 42
	R06	Andesite	22 34 35	46 07 18
Luncsoara	R09	Dacite	22 37 23	46 18 19
	R10	Andesite	22 37 20	46 17 36
Băiţa Bihor	R11	Andesite	22 37 33	46 29 58
Pietroasa	R12	Dacite	22 34 46	46 35 17
	R15	Dacite	22 39 30	46 32 43
	R21	Dacite	22 38 01	46 37 32
	R23	Dacite	22 35 25	46 36 47
	R24 fine-grained	Trachydacite (encl.)	22 35 25	46 36 47
	R24 coarse	Dacite	22 35 25	46 36 47
Budureasa	R27	Trachyandesite	22 34 48	46 40 01
	R28	Rhyolite	22 34 48	46 40 01
	R29	Trachyandesite	22 34 30	46 40 09
	R30	Basasaltic andesite	22 34 30	46 40 09
Vlădeasa	R34	Andesite	22 36 40	46 41 46
	R36	Dacite	22 37 23	46 42 33
	R39	Rhyolite	22 45 03	46 46 21
	R42	Dacite	22 46 14	46 49 50
	R43	Dacite	22 47 21	46 50 28
	R44	Dacite	22 48 17	46 51 31
	R46	Dacite	22 48 47	46 52 13
	R47	Rhyolite	22 35 50	47 01 32
	R50	Dacite	22 52 21	46 53 52
	R53	Dacite	22 52 21	46 53 52
	R54	Dacite	22 54 04	46 54 04
Dyke Gilau	R55	Dacite	23 11 40	46 36 37
Băişoara	R57	Dacite	23 27 30	46 35 17
	R61	Andesite	23 27 23	46 32 53
	R62	Andesite	23 27 23	46 32 53
	R63	Dacite	23 27 23	46 32 53
	R64	Dacite	23 27 23	46 32 53

The isotopic composition of Sr and Nd was measured on a selection of 11 samples covering the different intrusions of the Apuseni Mts. with an upgraded VG54E thermal ionization mass spectrometer (Clermont-Ferrand, France). Samples were dissolved by acid digestion (including dissolution of any refractory residue in pressurized PTFE vessels), and Sr, Sm and Nd fractions were separated by using extraction chromatographic methods adapted from Pin et al. (1994) and Pin and Santos Zalduegui (1997). Samples were loaded on a Ta single filament with a droplet of 3 M H_3PO_4, and the Sr isotope ratios were measured in dynamic triple collection mode, with normalization to $^{86}Sr/^{88}Sr = 0.1194$. After sample loading as a phosphate on single Ta filaments, Sm isotope ratios were measured in the single collection mode. The Nd separate was loaded on the side filaments of a triple Ta–Re–Ta assembly and analysed as the metal ion in dynamic triple collection mode, with normalization to $^{146}Nd/^{144}Nd = 0.7219$. Twenty-five analyses of the international NBS987 standard have given a Sr isotopic composition of 0.710248 ± 0.000026 (mean and standard deviation of 25 analyses). The French Ames Rennes Nd and the international JNdi-1 standards have given values of 0.511966 ± 0.000015 (eight analyses) and 0.512114 ± 0.000006 (six analyses), respectively (Table 3).

Results

Petrography and mineral composition

Our microscopic examination of the samples corroborates previous petrographic descriptions (e.g. Istrate 1978; Stefan et al. 1982, 1992). Samples collected in several discrete bodies display similar mineralogy and textures. The

Table 2 Major and trace element concentrations in the Apuseni Mts. whole-rock samples

Sample #	R04	R06	R09	R10	R11	R12	R15
SiO_2	64.28	57.27	61.78	56.53	55.04	65.38	65.32
TiO_2	0.54	0.80	0.67	0.74	1.08	0.60	0.49
Al_2O_3	15.20	15.73	15.79	16.34	15.33	15.09	14.93
Fe_2O_3t	3.77	6.77	5.85	7.62	8.15	3.93	4.21
MnO	0.09	0.12	0.11	0.13	0.12	0.10	0.07
MgO	1.75	5.08	2.78	4.08	5.33	1.33	1.88
CaO	3.75	6.55	4.66	6.67	7.78	3.28	3.50
Na_2O	3.95	3.40	3.04	3.00	1.03	3.66	3.29
K_2O	2.68	2.26	3.49	2.64	3.19	3.79	3.52
P_2O_5	0.15	0.23	0.24	0.28	0.28	0.17	0.16
LOI	2.88	0.78	1.47	1.07	1.78	1.85	1.63
Total	99.02	98.97	99.87	99.11	99.11	99.18	98.99
U	3.6	3.1	6.1	2.0	1.8	3.9	2.3
Th	14	11	10	7.2	7.2	14	12
Zr	161	180	144	118	130	207	130
Hf	5.0	4.4	3.6	3.4	3.2	5.4	3.3
Nb	12	12	7.8	4.9	7.5	11	6.1
Ta	1.4	1.0	0.7	0.5	0.5	0.9	0.6
Ba	586	448	619	627	507	728	682
Rb	94	81	123	80	108	137	121
Sr	341	543	433	585	450	286	345
Cs	3.1	3.0	7.4	4.3	15.3	6.5	4.1
Ga	20	21	20	21	20	20	18
V	72	122	151	187	206	65	87
Cr	39	141	39	35	80	17	34
Co	8.4	32	16	26	22	7.7	10
Ni	13	91	9.0	14	16	8.2	9.2
Zn	53	59	73	89	88	55	37
Pb	26	15	22	29	8	35	17
La	26	28	27	25	25	35	26
Ce	47	53	49	49	50	66	47
Pr	5.9	6.9	7.0	6.3	6.6	8.2	5.5
Nd	21	25	26	23	25	28	19
Sm	4.6	5.4	5.4	5.0	5.7	5.3	3.9
Eu	1.5	1.5	1.4	1.5	1.5	1.4	0.8
Gd	4.0	4.9	5.0	4.6	5.1	4.9	3.3
Tb	0.59	0.72	0.73	0.63	0.77	0.77	0.47
Dy	3.8	4.3	4.2	3.8	4.5	4.5	3.1
Ho	0.85	0.91	0.90	0.80	0.90	0.91	0.65
Er	2.5	2.4	2.4	2.2	2.3	2.5	1.8
Tm	0.38	0.38	0.36	0.33	0.34	0.39	0.28
Yb	2.6	2.4	2.4	2.1	2.1	2.5	1.7
Lu	0.40	0.35	0.40	0.30	0.31	0.37	0.30
Y	21	25	25	23	26	28	20
Apatite T (°C)	879	844	907	860	837	911	901
Zircon T (°C)	704	649	678	622	622	730	690

Table 2 continued

Sample #	R21	R23	R24 fine	R24 coarse	R27	R28	R29
SiO_2	66.43	66.60	63.06	66.80	55.07	69.87	55.88
TiO_2	0.62	0.60	0.92	0.62	1.16	0.42	1.29
Al_2O_3	15.39	14.98	15.93	15.31	18.61	13.97	19.15
Fe_2O_3t	3.86	3.71	5.32	3.48	6.94	2.85	6.53
MnO	0.08	0.08	0.13	0.07	0.10	0.05	0.09
MgO	1.24	1.12	1.29	1.13	2.66	0.66	2.65
CaO	2.78	2.90	3.21	2.97	5.99	1.04	5.28
Na_2O	3.84	3.69	4.46	3.79	4.08	3.16	4.09
K_2O	4.02	3.85	3.62	3.82	2.32	5.73	2.91
P_2O_5	0.17	0.17	0.33	0.16	0.46	0.12	0.54
LOI	1.03	2.00	1.02	1.01	1.45	1.70	1.55
Total	99.47	99.70	99.29	99.16	98.84	99.56	99.97
U	2.7	3.0	6.1	2.6	1.5	3.7	2.0
Th	15	14	18	13	11	16	7.5
Zr	208	213	287	218	211	185	1364
Hf	5.5	5.6	7.5	6.2	17	4.6	27
Nb	12	12	18	11	10	13	7.2
Ta	1.0	1.0	1.6	0.9	0.5	1.1	0.5
Ba	724	729	723	790	1514	647	2470
Rb	146	142	143	129	74	250	88
Sr	244	228	266	264	597	210	560
Cs	5.6	5.7	5.3	5.1	4.3	7.6	2.7
Ga	19	18	22	19	23	16	29
V	66	65	48	55	93	32	65
Cr	17	10	10	12	13	10	10
Co	7.7	10	11	9.7	12	7.0	15
Ni	4.8	6.1	5.2	5.2	6.3	4.4	6.7
Zn	50	64	66	55	64	39	94
Pb	26	34	27	29	16	23	23
La	33	37	38	36	27	35	30
Ce	67	71	79	73	56	65	57
Pr	7.7	8.6	9.9	8.8	6.8	7.3	7.7
Nd	28	32	38	31	26	23	28
Sm	5.3	6.0	8.3	5.8	5.4	4.0	5.8
Eu	1.3	1.4	1.9	1.5	2.2	0.8	2.2
Gd	5.3	5.7	7.8	5.3	4.8	3.8	5.4
Tb	0.78	0.90	1.26	0.79	0.71	0.57	0.67
Dy	4.9	5.5	7.4	4.9	4.3	3.5	4.4
Ho	1.04	1.12	1.60	0.98	0.91	0.75	0.90
Er	2.9	3.0	4.1	2.8	2.7	2.1	2.7
Tm	0.41	0.46	0.64	0.41	0.39	0.30	0.43
Yb	2.7	3.1	4.3	2.8	2.7	2.0	2.9
Lu	0.43	0.47	0.64	0.39	0.43	0.34	0.50
Y	32	32	45	30	26	24	28
Apatite T (°C)	923	921	962	920	903	919	940
Zircon T (°C)	739	741	752	744	692	752	922

Table 2 continued

Sample #	R30	R34	R36	R39	R42	R43	R44
SiO_2	52.05	56.85	64.92	71.25	65.99	65.78	62.82
TiO_2	1.47	1.08	0.53	0.41	0.51	0.50	0.74
Al_2O_3	18.16	18.18	15.55	14.04	15.16	15.41	15.60
Fe_2O_3t	9.11	6.81	4.41	2.47	4.48	4.06	5.42
MnO	0.18	0.11	0.08	0.06	0.08	0.07	0.10
MgO	4.00	2.84	1.43	0.69	1.61	1.63	2.17
CaO	7.61	4.59	3.99	1.84	3.41	3.41	4.28
Na_2O	3.27	3.77	3.81	3.65	3.85	3.94	3.84
K_2O	1.80	2.19	2.58	4.10	2.67	2.76	2.45
P_2O5	0.28	0.32	0.13	0.11	0.12	0.13	0.18
LOI	1.38	2.55	1.42	1.00	1.29	1.13	1.99
Total	99.32	99.31	98.86	99.61	99.18	98.82	99.58
U	1.4	1.7	3.9	4.6	3.7	2.6	3.3
Th	6.5	7.4	11	17	13	12	10
Zr	357	469	179	162	192	164	165
Hf	7.9	11	5.1	4.4	5.1	4.8	4.4
Nb	5.5	15	12	12	12	11	10
Ta	0.5	0.7	1.0	1.0	1.0	0.9	1.8
Ba	768	1100	591	689	654	616	588
Rb	71	77	93	163	97	103	94
Sr	639	511	253	169	212	232	267
Cs	5.1	2.9	4.5	5.7	5.2	6.4	4.0
Ga	29	30	20	18	21	20	21
V	160	106	72	33	62	76	108
Cr	36	37	23	12	18	16	28
Co	22	18	16	7.0	11	12	16
Ni	12	16	9.0	2.6	10	7.5	12
Zn	99	96	62	35	70	57	66
Pb	10	15	23	24	21	19	15
La	17	34	26	30	32	30	24
Ce	40	69	54	66	63	54	50
Pr	5.2	8.6	6.5	7.2	7.8	7.0	6.8
Nd	19	33	23	28	28	21	23
Sm	4.6	7.1	4.5	5.2	5.3	4.3	5.2
Eu	1.9	2.4	1.2	1.3	1.1	1.2	1.3
Gd	4.1	6.4	4.5	4.9	4.6	4.1	5.0
Tb	0.64	0.98	0.77	0.78	0.76	0.71	0.78
Dy	4.0	5.8	4.9	5.0	4.7	4.3	4.7
Ho	0.83	1.21	1.03	1.05	0.99	0.89	0.92
Er	2.4	3.2	2.9	3.1	3.0	2.6	2.7
Tm	0.38	0.48	0.46	0.45	0.43	0.40	0.38
Yb	2.6	3.2	2.8	3.0	2.7	2.6	2.7
Lu	0.40	0.46	0.42	0.41	0.42	0.40	0.39
Y	22	32	28	31	30	27	29
Apatite T (°C)	794	881	875	921	882	881	884
Zircon T (°C)	711	819	717	734	732	716	699

Table 2 continued

Sample #	R46	R47	R50	R53	R54	R55	R57
SiO_2	61.13	81.89	64.63	67.16	66.83	65.11	62.76
TiO_2	0.57	0.09	0.54	0.46	0.49	0.49	0.57
Al_2O_3	16.96	10.34	15.74	15.31	15.19	15.18	15.69
Fe_2O_3t	5.62	0.26	4.61	3.70	3.86	3.75	4.58
MnO	0.10	0.01	0.08	0.05	0.07	0.06	0.08
MgO	1.83	0.03	2.10	1.48	1.52	1.78	2.73
CaO	4.70	0.17	3.77	3.54	2.79	3.16	4.55
Na_2O	4.54	0.15	4.26	3.23	4.25	3.44	3.26
K_2O	2.11	2.91	2.36	3.30	3.18	3.26	2.97
P_2O_5	0.15	0.15	0.13	0.16	0.13	0.13	0.16
LOI	1.33	3.28	1.55	1.47	1.39	3.56	2.31
Total	99.04	99.28	99.77	99.86	99.69	99.92	99.67
U	2.5	4.6	3.5	4.8	3.6	3.5	4.3
Th	9.1	9.0	10	14	15	15	13
Zr	241	57	158	132	165	131	124
Hf	6.1	1.7	4.7	4.0	4.4	3.8	3.4
Nb	13	18	12	13	11	12	11
Ta	0.8	1.9	0.8	1.3	0.9	1.1	1.2
Ba	660	878	527	659	566	586	605
Rb	71	86	77	117	114	125	89
Sr	304	321	240	312	220	241	367
Cs	2.7	0.7	3.2	3.7	2.8	6.5	2.0
Ga	25	12	20	20	18	19	19
V	63	10	73	55	56	66	92
Cr	14	10	21	19	18	10	52
Co	13	3.0	9.5	4.9	9.8	8.3	11
Ni	9.2	0.2	10	5.0	6.7	6.4	11
Zn	75	12	45	42	46	47	53
Pb	21	17	18	17	23	23	14
La	29	10	25	29	28	24	30
Ce	61	19	50	55	55	48	58
Pr	7.9	2.6	6.3	6.9	6.5	5.8	6.9
Nd	29	7	22	22	22	18	23
Sm	6.6	1.4	4.4	4.0	4.1	3.3	3.8
Eu	1.6	0.5	1.1	1.1	1.0	0.9	0.9
Gd	6.4	2.2	4.0	3.4	3.9	3.1	3.4
Tb	1.04	0.47	0.68	0.54	0.65	0.50	0.55
Dy	6.5	3.5	4.5	3.2	4.0	3.0	3.2
Ho	1.31	0.82	0.96	0.62	0.85	0.61	0.66
Er	3.7	2.5	2.7	1.7	2.5	1.7	1.8
Tm	0.52	0.40	0.39	0.25	0.37	0.27	0.26
Yb	3.5	2.5	2.5	1.7	2.3	1.8	1.8
Lu	0.51	0.34	0.37	0.22	0.33	0.25	0.28
Y	37	27	27	20	27	20	20
Apatite T (°C)	843	1051	875	923	897	880	875
Zircon T (°C)	727	748	704	701	718	701	673

Table 2 continued

Sample #	R61	R62	R63	R64
SiO_2	60.39	55.78	67.25	61.19
TiO_2	0.57	0.73	0.43	0.77
Al_2O_3	15.71	15.86	14.85	15.36
Fe_2O_3t	5.20	8.58	3.66	6.08
MnO	0.09	0.19	0.09	0.10
MgO	3.75	4.12	1.31	2.95
CaO	5.45	6.60	2.61	4.69
Na_2O	2.95	3.48	4.04	3.20
K_2O	1.78	2.11	3.38	2.68
P_2O_5	0.16	0.36	0.11	0.23
LOI	3.55	1.62	1.22	1.62
Total	99.60	99.43	98.95	98.87
U	3.2	6.2	3.9	5.2
Th	12	14	15	13
Zr	121	170	179	168
Hf	3.2	5.0	4.8	4.8
Nb	10	13	12	15
Ta	0.7	1.3	0.9	1.3
Ba	597	483	664	593
Rb	54	94	121	127
Sr	336	322	182	296
Cs	1.6	2.8	4.3	4.0
Ga	21	22	19	22
V	131	178	48	109
Cr	96	33	14	82
Co	17	26	3.2	16
Ni	11	24	4.9	10
Zn	68	87	72	60
Pb	34	14	27	13
La	28	71	30	34
Ce	57	161	61	72
Pr	6.5	20	7.4	8.7
Nd	23	77	24	32
Sm	4.1	15	5.0	6.7
Eu	1.1	2.1	1.1	1.0
Gd	3.4	11	4.5	5.9
Tb	0.54	1.6	0.73	0.86
Dy	3.2	8.6	4.6	5.2
Ho	0.64	1.7	0.97	1.01
Er	1.7	4.4	2.8	2.9
Tm	0.27	0.67	0.42	0.40
Yb	1.6	4.3	2.9	2.6
Lu	0.23	0.64	0.42	0.36
Y	19	50	30	32
Apatite T (°C)	843	882	883	893
Zircon T (°C)	668	642	729	694

Table 3 Whole-rock Rb–Sr and Sm–Nd isotopic data

Sample #	Rb (ppm)	Sr (ppm)	$^{87}Rb/^{86}Sr$	$^{87}Sr/^{86}Sr$	2 s.e.	$^{87}Sr/^{86}Sr_{80}$	Sm (ppm)	Nd (ppm)	$^{147}Sm/^{144}Nd$	$^{143}/^{144}Nd$	2 s.e.	$(^{143}Nd/^{144}Nd_{80})^{*}$	$(\varepsilon_{Nd80})^{**}$
R06	81	543	0.43	0.705066	11	0.70458	5.4	27	0.1223	0.512683	8	0.51262	1.6
R10	80	585	0.40	0.707469	17	0.70702	4.91	22.5	0.1320	0.512531	8	0.51246	−1.4
R11	108	450	0.69	0.706317	16	0.70553	6.34	30	0.1265	0.512561	7	0.51249	−0.8
R21	146	244	1.73	0.708449	17	0.70648	6.09	30	0.1232	0.512495	7	0.51243	−2.0
R27	74	597	0.36	0.706750	18	0.70634	6.06	29.7	0.1234	0.512530	7	0.51247	−1.4
R39	163	169	2.79	0.709487	16	0.70631	5.56	28.2	0.1192	0.512490	7	0.51243	−2.1
R44	94	267	1.02	0.707916	16	0.70676	5.1	23.6	0.1302	0.512542	7	0.51247	−1.2
R46	71	304	0.68	0.707504	18	0.70674	7.05	31.6	0.1349	0.512498	7	0.51243	−2.1
R50	77	240	0.93	0.707672	19	0.70662	4.72	28.1	0.1016	0.512550	7	0.51250	−0.7
R54	114	220	1.50	0.708273	37	0.70657	4.6	23	0.1212	0.512520	7	0.51246	−1.5
R62	94	322	0.84	0.707910	16	0.70695	14.9	34	0.2650	0.512484	6	0.51235	−3.7

* λ ^{147} Sm= 6.54×10^{-12} y^{-1} (Steiger and Jäger 1977). ** Present-day ($^{147}Sm/^{144}Nd$) CHUR and ($^{143}Nd/^{144}Nd$)CHUR = 0.1966 and 0.512638, respectively (Jacobsen and Wasserburg 1980). The present-day $^{87}Sr/^{86}Sr$ ratios were corrected for in situ decay of ^{87}Rb since igneous emplacement at 80 Ma using Rb and Sr concentrations determined by X-ray fluorescence. For Nd, the age-corrected values given by the ε-notation were calculated with the $^{147}Sm/^{144}Nd$ ratios measured by X-ray fluorescence

main rock-forming minerals are plagioclase, K-feldspar, quartz, amphibole and biotite. Opaques (magnetite, ilmenite, pyrite and chalcopyrite), apatite, zircon and titanite are ubiquitous accessory phases. Relic cores of clinopyroxene (augite to diopside (Morimoto 1989): Mg# = 0.73–0.85) (see Supplementary Material S1a) were frequently observed in the amphibole which is itself locally surrounded by biotite (Fig. 3a). Plagioclase usually occurs as strongly zoned phenocrysts with cores of labradorite and rims of oligoclase with the exception of sample R30 in which a core of bytownite (An_{83}) has been analysed (see Supplementary Material S1b). Plagioclase is mostly euhedral to hypidiomorphic, but crystals with higher aspect ratio also occur (sample R13). In porphyritic samples, smaller grains of plagioclase are present in the groundmass (Fig. 3b). Plagioclase contains some inclusions of amphibole, opaques and apatite as well as some rare zircon. K-feldspar is usually anhedral, locally perthitic and surrounding grains of plagioclase, opaques, apatite and biotite. K-feldspar is rich in orthose (Or_{82} to Or_{96}) with a few core analyses ranging from Or_{60} to Or_{70} (see Supplementary Material S1c). At the contact with K-feldspar, plagioclase frequently displays partly corroded contours. Quartz is anhedral and fills the interstices between the other minerals. Amphibole, a magnesiohornblende (Leake et al. 2004) with a Mg# ranging between 0.64 and 0.82 (see Supplementary Material S1d), is usually hypidiomorphic (Fig. 3c), very locally included in plagioclase or displaying interstitial contacts with plagioclase phenocrysts. Biotite (Fe# = 0.27–0.64, moderate Ti content: 0.43–0.76 p.f.u.) (see Supplementary Material S1e) is hypidiomorphic to anhedral (Fig. 3d) and locally fills the voids between feldspars and amphibole. Small grains of biotite frequently surround the amphibole. Euhedral grains of apatite are ubiquitous as well as apatite needles dispersed in other minerals. Titanite usually surrounds opaque minerals and is not abundant. In volcanic facies, the matrix is microcrystalline to vitreous. These petrographic observations suggest early crystallization of apatite and opaques followed by plagioclase and clinopyroxene. Amphibole seems to have formed by reaction from the clinopyroxene and was earlier than biotite. K-feldspar and quartz are late crystallizing phases.

The extent of alteration varies among the different samples with some displaying deep alteration and others being totally fresh. Only weakly to non-altered samples have been considered for the geochemistry. Hornblende is transformed into an assemblage of fibrous amphibole (actinote), epidote, secondary biotite and chlorite. Biotite is frequently altered to chlorite and epidote. Alteration is also expressed by damouritization of feldspars. Pronounced alteration into carbonates was noted in sample R20. The microcrystalline groundmass is locally cut by fissures made of calcite, epidote and quartz.

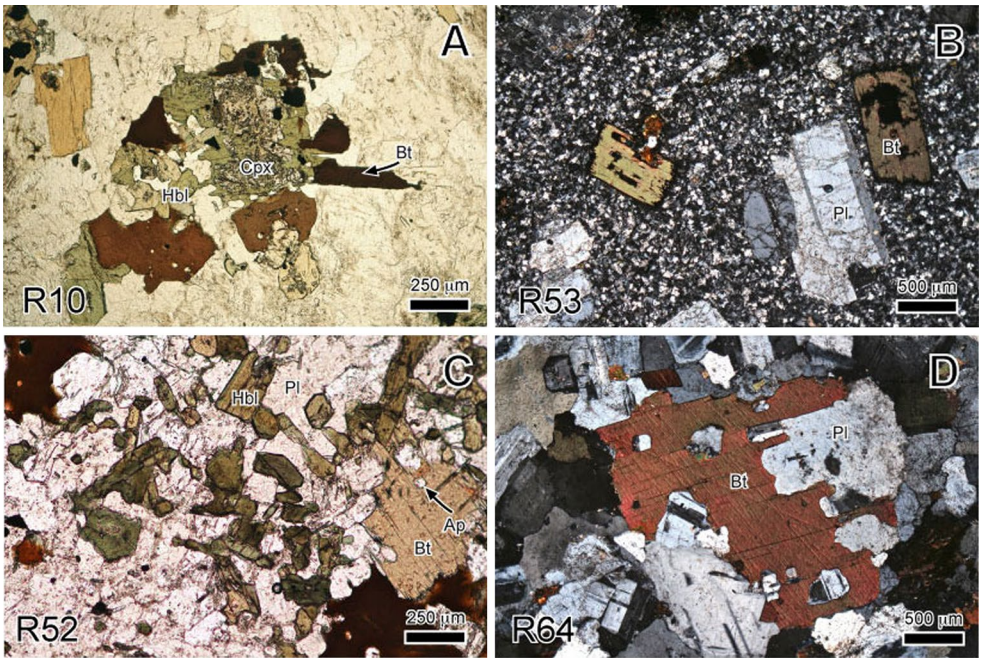

Fig. 3 Microphotographic pictures of selected samples from the Late Cretaceous magmatic rocks of the Apuseni Mountains. **a** Sample R10 (Luncsoara) displaying relic cores of clinopyroxene (Cpx) within the amphibole (Hbl) which is itself surrounded by biotite (Bt) (plane-polarized light). **b** Sample R53 (Vlădeasa) is porphyritic with large phenocrysts of plagioclase (Pl) and biotite (Bt) (crosspolarized light). **c** Sample R52 (Vlădeasa) displaying hypidiomorphic amphibole (Hbl) in contact with plagioclase (Pl). Please note the apatite grain (Ap) included in biotite (Bt) (plane-polarized light). **d** Sample R64 (Băişoara) with biotite (Bt) displaying interstitial contours surrounding plagioclase (crosspolarized light)

Geochemistry

In the TAS diagram (Fig. 4a), samples from the Apuseni Mts. plot in the fields of basaltic andesites to rhyolites with some samples, higher in K_2O, in the fields of basaltic trachyandesites to trachytes. Most of the samples plot just below the limit between the alkaline and subalkaline series (Miyashiro 1978). The whole trend is calc-alkaline in the AFM (Fig. 4b) and MALI (Frost et al. 2001) (Fig. 4c) diagrams and more precisely, medium- to high-K in the K_2O–SiO_2 diagram of Peccerillo and Taylor (1976) (Fig. 4d). The Apuseni trend is magnesian in the Frost and Frost (2008) classification (Fig. 4e). Our data overlap with previous results (Istrate 1978; Stefan 1980; Stefan et al. 1982, 1992).

In the Harker diagrams (Fig. 5), samples from the different intrusions display overlapping trends of decreasing FeO_t, MgO, CaO, TiO_2 and P_2O5 and increasing K_2O with increasing $SiO_2{\cdot}Na_2O$ remains relatively constant (not shown). The mafic dykes analysed by Istrate (1978), Stefan (1980) and Stefan et al. (1982) overlap in composition with the least differentiated samples and are similar to the calc-alkaline dykes associated with the late Alpine intrusions (e.g. Traversella, Biella, Bergell, Adamello) (Dal Piaz et al. 1979; Venturelli et al. 1984; von Blanckenburg et al. 1992; Bogaerts 1998; Bogaerts and Vander Auwera 1999; Peccerillo and Martinotti 2006) (Fig. 5).

Samples from the different massifs have similar trace element contents (Fig. 6). Among trace elements, Sr, Zn, V, Ga and Ni (not shown) decrease with differentiation, whereas Rb and Th increase and Ba and Zr are rather constant. Two samples from Budureasa (R27 and R29) display higher Ba content than the main trend suggesting some accumulation of biotite and/or K-feldspar, the main Ba carriers in the samples. Three samples (R29, R30 and R34) have significantly higher Zr content than the main trend suggestive of some zircon accumulation. Chondrite-normalized REE patterns (Fig. 7) display LREE fractionation [(La/Yb)N = 3.9–17.4 with an average of 11.7] and negative to slightly positive Eu anomaly ($(Eu/Eu^*)_N = Eu_N/(\sqrt{(Sm_N{*}Gd_N)}) = 0.51–1.34$). Compared to N-MORB in spiderdiagrams (Fig. 8), the Apuseni samples are enriched in incompatible elements (K, Rb, Ba, Th, LREE) and display negative anomalies in Nb, Ta and Ti. The Apuseni samples plot in the volcanic arc field (VAG) in the Pearce et al. (1984) discrimination diagrams (Fig. 9a–d) and partly overlap in composition with arc magmas in the Th/Yb and Nb/Yb diagram of Pearce and Peate (1995) (Fig. 9e).

Sr and Nd isotopic data of the Apuseni samples have been recalculated back to an age of 80 Ma in agreement with the Re–Os geochronological data on the Mo-Cu skarn associated with the Băiţa Bihor granodiorite (Zimmerman et al. 2008). In the ε_{Ndt} versus $(^{87}Sr/^{86}Sr)_{80}$ (Fig. 10a), samples from the

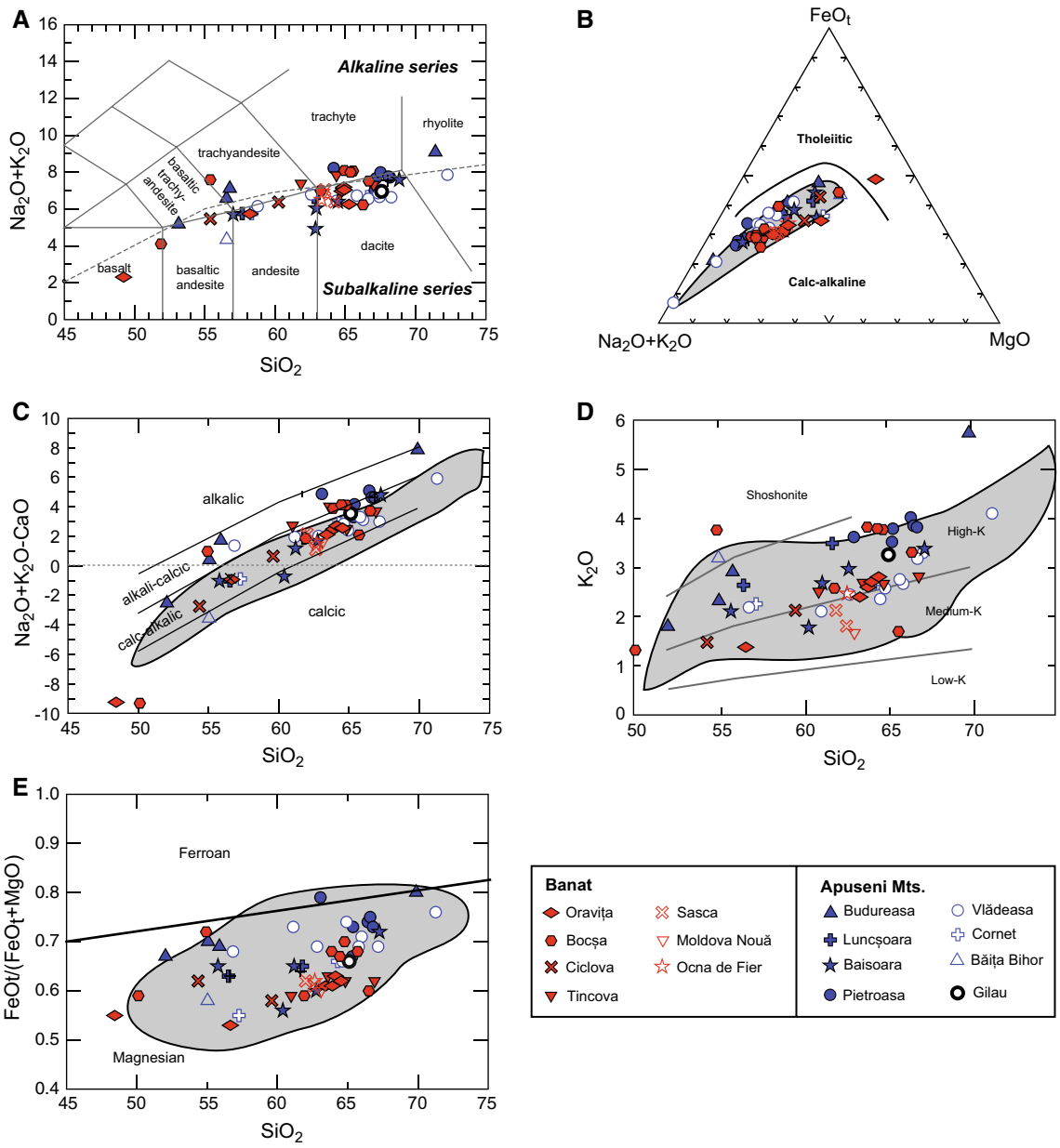

Fig. 4 Nomenclature of the Late Cretaceous igneous rocks from the Apuseni Mts. and Banat. **a** TAS diagram: analyses have been recalculated to 100 % on a volatile free basis, and Fe is considered as total wt% Fe_2O_3 (Le Maitre 1989). Discrimination between the alkaline and subalkaline fields has been made with the boundary line proposed by Miyashiro (1978). **b** AFM diagram showing the boundary between the calc-alkaline and tholeiitic fields from Irvine and Baragar (1971). **c** MALI index from Frost et al. (2001). **d** Subdivision of the calc-alkaline rocks in the K_2O versus silica diagram with the boundary lines from Peccerillo and Taylor (1976). **d** Ferroan versus magnesian series from Frost and Frost (2008). *Grey fields* are data on the Late Cretaceous igneous rocks from the Apuseni Mts. from Istrate (1978), Stefan (1980), Stefan et al. (1982) and Stefan et al. (1992). Data for the Late Cretaceous magmatic rocks of Banat are from Dupont et al. (2002)

Apuseni display mildly negative epsilon Nd (−1 to −4) and relatively low Sr initial ratios (0.7055–0.7070) except one sample from the Cornet intrusion which has a positive epsilon Nd (2) and lower $(^{87}Sr/^{86}Sr)_{80}$ (0.7046). These Sr isotopic data agree with previous results of Pavelescu et al. (1985) (initial $^{87}Sr/^{86}Sr$ of 0.708) reported by Stefan et al. (1992). These data imply source materials that on a time-integrated basis were both weakly enriched to slightly depleted (Cornet sample) in LREE and in Rb relative to Sr.

Barometry and thermometry of the Apuseni samples

P_2O_5 is decreasing with differentiation (Fig. 5) indicating that apatite, an ubiquitous accessory mineral, is a

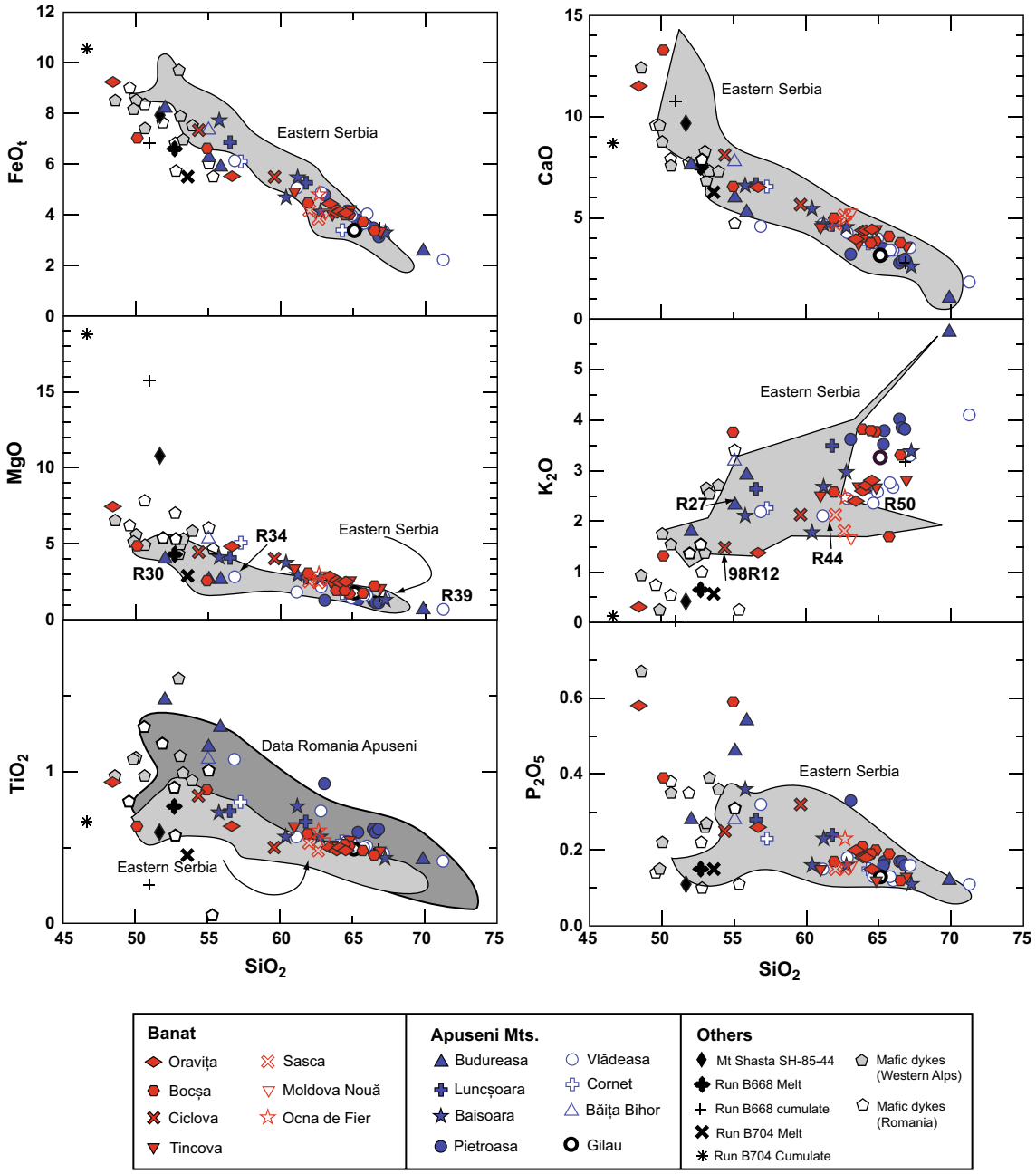

Fig. 5 Variation diagrams of major elements displaying data for the Late Cretaceous igneous rocks of the Apuseni Mts. and Banat (data from Dupont et al. 2002). Data of Kolb et al. (2013) for the Late Cretaceous igneous rocks of Eastern Serbia are shown as *light grey fields*. Data for the mafic dykes (calc-alkaline) are from Dal Piaz et al. (1979), Venturelli et al. (1984), von Blanckenburg et al. (1992), Bogaerts (1998), Bogaerts and Vander Auwera (1999) and Peccerillo and Martinotti (2006) for the western alpine intrusions and from Istrate (1978), Stefan (1980) and Stefan et al. (1982) for the Apuseni Mts. Data for SH-85-44 as well as experimental melts and cumulates (Run B668 and B704) are from Müntener et al. (2001). See text for explanation

fractionating phase. On the contrary, Zr remains rather constant. In agreement with these observations, apatite (792 to 1075 °C) (Harrison and Watson 1984) and zircon (622 to 752 °C) (Watson and Harrison 1983) saturation temperatures indicate their, respectively, early and late crystallization (Table 2). The Al-in hornblende geobarometer of Johnson and Rutherford (1989) was used on the plutonic samples and confirms the shallow level of emplacement of the intrusions (<0.2 GPa) (see Supplementary Material S4).

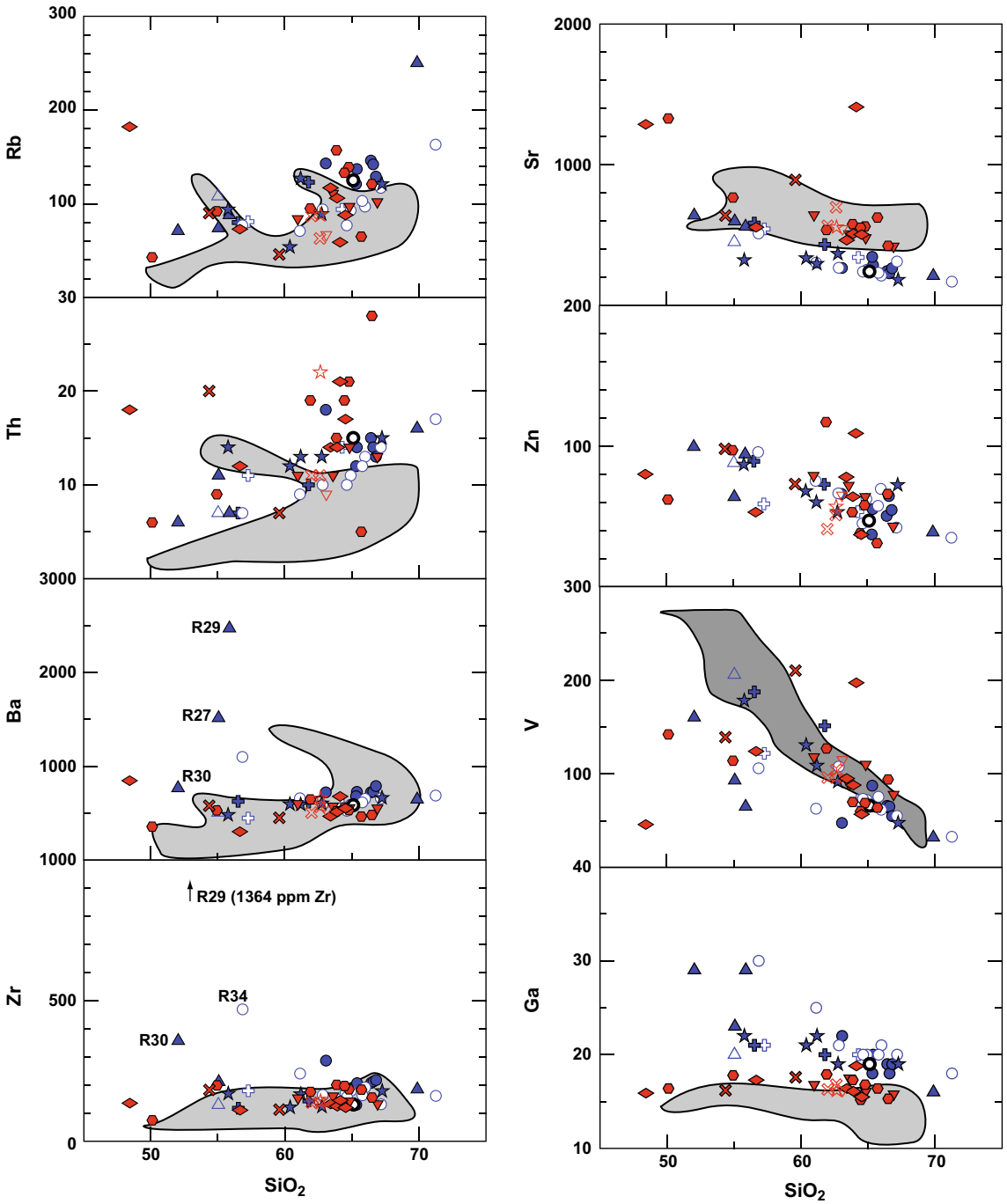

Fig. 6 Variation diagrams of selected trace elements displaying data for the Late Cretaceous igneous rocks of the Apuseni Mts. and Banat (data from Dupont et al. 2002). Data of Kolb et al. (2013) for the Late Cretaceous igneous rocks of Eastern Serbia are shown as *grey fields*. Same *symbols* as in Fig. 4

Comparison with other Late Cretaceous igneous rocks from the Banatitic belt and with Alpine intrusions

The major element composition of our samples from the Apuseni Mts. is overlapping with the composition of samples from Banat (Dupont et al. 2002) and from Eastern Serbia (Timok and Ridanj-Krepoljin) (Kolb et al. 2013) with, however, a tendency towards slightly higher TiO_2 content in the Apuseni samples (Figs. 4, 5). Samples from the different regions have overlapping FeOt/MgO (Fig. 4b), but samples from the Apuseni have a slightly higher FeOt/MgO than samples from Banat.

Samples from Romania (Apuseni, Banat) and Serbia display similar spiderdiagrams (Fig. 8) and REE patterns

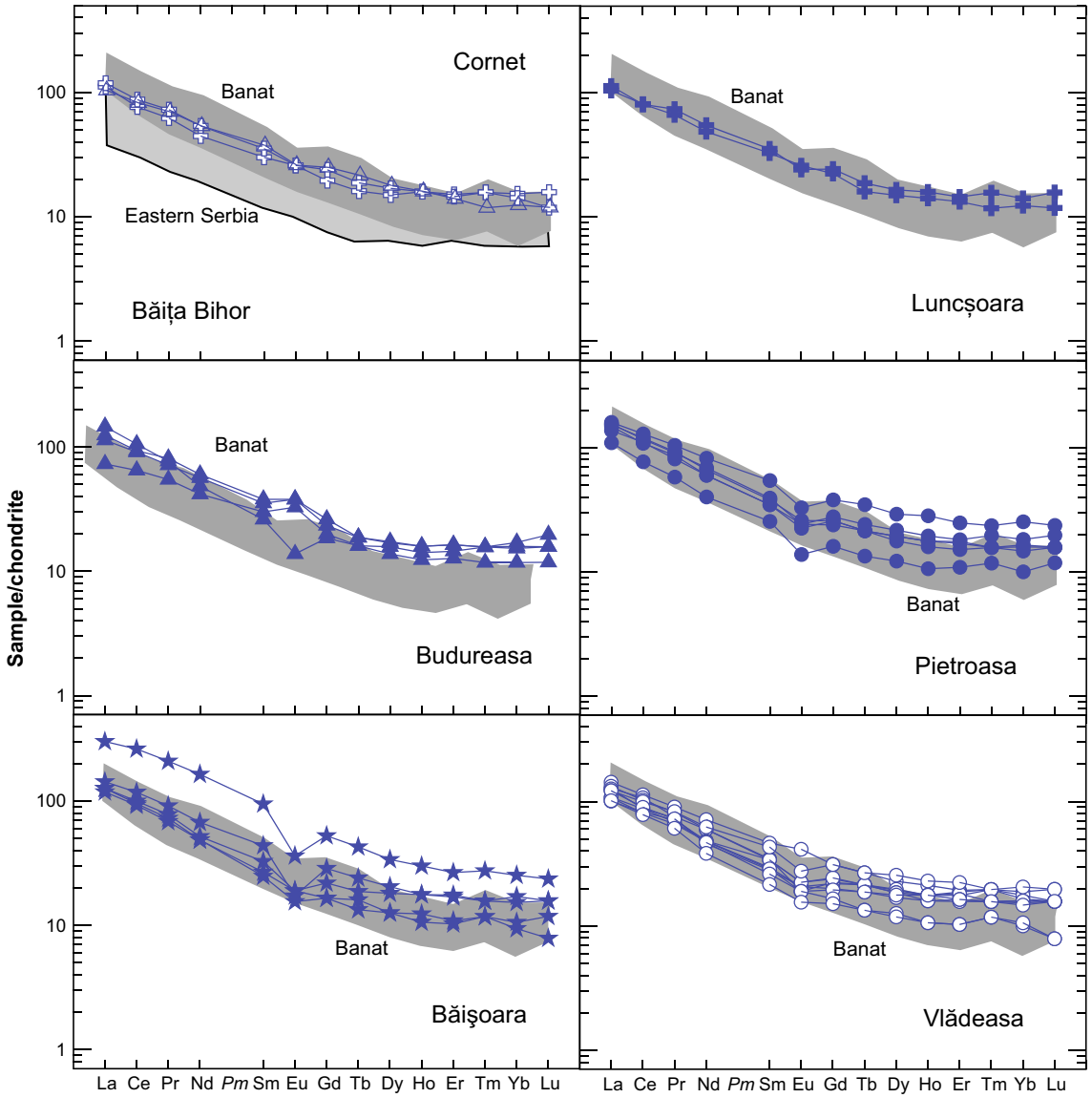

Fig. 7 REE patterns normalized to the C1 chondrite of Sun and McDonough (1989) of the Late Cretaceous igneous rocks of the Apuseni Mts. Data for Banat (Dupont et al. 2002) and Eastern Serbia (Kolb et al. 2013) are shown as *grey fields*

(Fig. 7). However, samples from Serbia are generally lower in U, Th, Zr, Hf, Nb, Ta and LREE (Figs. 6, 8) than samples from Romania. Interestingly, samples from the three regions mostly differ by their Ga and also Sr contents. The Ga content decreases from the Apuseni to Banat and then Serbia, but the least differentiated samples from Banat and Serbia have similar Ga content, whereas the Sr content is lower in the Apuseni trend than in the Banat and Serbia trends. These differences are better observed in a Ga versus Sr diagram (Fig. 11).

Kolb et al. (2013) recognized that a series of samples from Serbia are characterized by high Sr/Y ratios and low Y contents and thus have adakite-like signatures (Defant and Kepezhinskas 2001). This is not observed in the Romanian samples as Sr/Y is lower than 40 except in four samples from Banat, La/Yb is lower than 20 and Y is higher than 18 except in a few samples of Banat.

Samples from Banat and Apuseni have significantly different isotopic composition. In the ε_{Ndt} versus $(^{87}Sr/^{86}Sr)_{80}$ diagram (Fig. 10a), samples from Banat have higher ε_{Ndt} (0–+4) and lower $(^{87}Sr/^{86}Sr)_{80}$ (0.7042–0.7058) than the Apuseni samples (ε_{Ndt} (−0.7 to −3.7), $(^{87}Sr/^{86}Sr)_{80}$ (0.70553–0.70702)). Note that the sample from the Cornet intrusion (Apuseni Mts.) ($\varepsilon_{Ndt} = 1.6$, $(^{87}Sr/^{86}Sr)_{80} = 0.70458$) plots in the field of the Banat samples. The isotopic composition of samples from Serbia overlaps with that of samples from Banat (Fig. 10b).

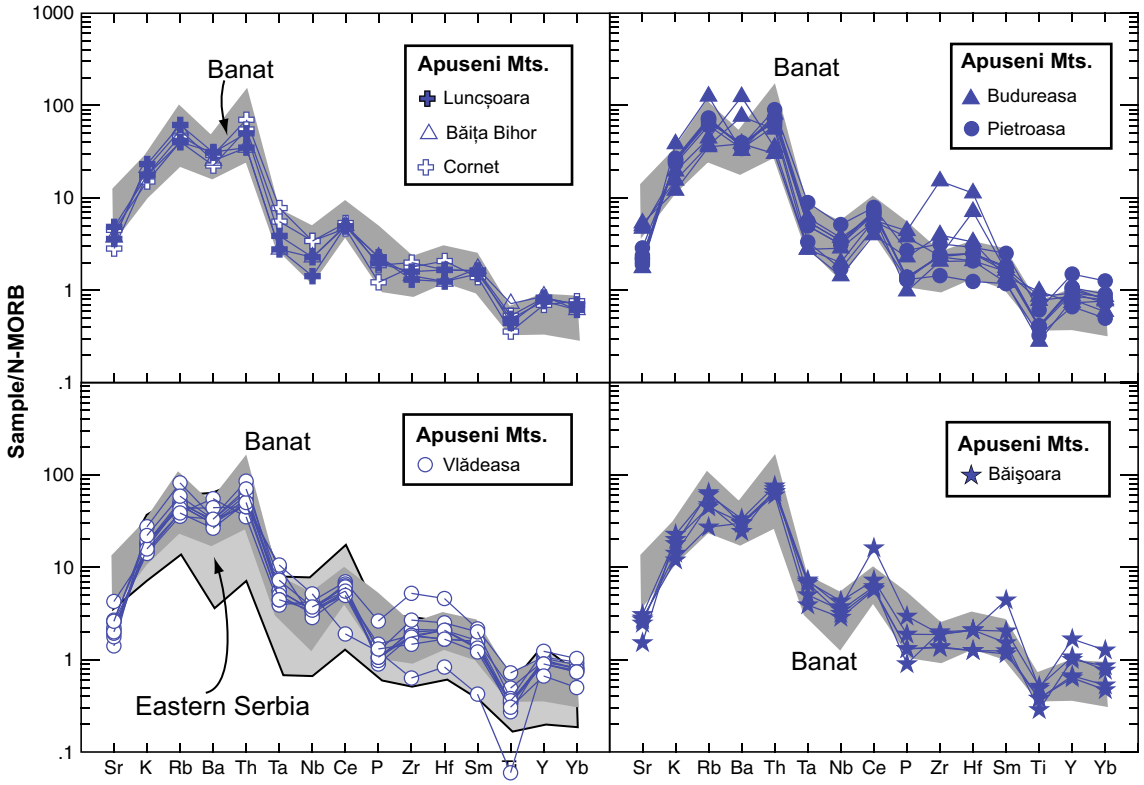

Fig. 8 Spiderdiagrams normalized to MORB (Pearce 1983) of the Late Cretaceous igneous rocks of the Apuseni Mts. Data for Banat (Dupont et al. 2002) and Eastern Serbia (Kolb et al. 2013) are shown as *grey fields*

As shown in Supplementary Materials Fig 1 and Fig 2, the Apuseni and Banat samples are similar in major and trace element composition to the Adamello and Bergell intrusions from the Alps.

Discussion

Differentiation processes within the Apuseni Mts. trend

Samples from the Apuseni Mts. have been collected in different intrusions/extrusions, but their comparable major and trace element compositions suggest that they differentiated from a similar parent magma. Consequently, in order to constrain the differentiation process(es), we selected samples from the Vlădeasa volcanics and Budureasa pluton because the largest series of samples is available from the former and the latter contains the least differentiated sample and is also close to Vlădeasa.

Mixing between the least and most differentiated magmas is a possible differentiation process as mingling between a microdioritic and a granodioritic facies has been observed in the Pietroasa intrusion. The mixing process has been tested with two sets of samples: samples R34 (56.85 wt% SiO_2) (mafic end member), R39 (71.25 wt% SiO_2) (acid end member) and R50 (64.63 wt% SiO_2) (intermediate facies) as well as samples R30 (52.05 wt% SiO_2) (mafic end member), R39 (71.25 wt% SiO_2) (acid end member) and R44 (62.82 wt% SiO_2) (intermediate facies). These compositions were selected because, in variation diagrams, they plot on the differentiation trends, thus providing the most favourable cases to test the mixing process. All major and trace elements have been considered in the test. The procedure proposed by Fourcade and Allègre (1981) was used:

$$x = \frac{\left(C^i_{\text{mix}} - C^i_{\text{fels}}\right)}{\left(C^i_{\text{maf}} - C^i_{\text{fels}}\right)}$$

where x fraction of the mafic component, C^i_{mix} the concentration of element i in the intermediate sample, C^i_{fels} the concentration of element i in the felsic end member of the mixing and C^i_{maf} the concentration of element i in the mafic end member of the mixing.

In a C_{mix}–C_{fels} versus C_{maf}–C_{fels} diagram, the differentiation trend can be predicted by a mixing process if a good-fit regression line with a slope (=x, the fraction of the mafic component) between 0 and 1 can be drawn through the origin (Fig. 12). For both sets of samples, Ba, Zr, Sr and to a lesser extent Zn, V, Rb plot outside of a possible

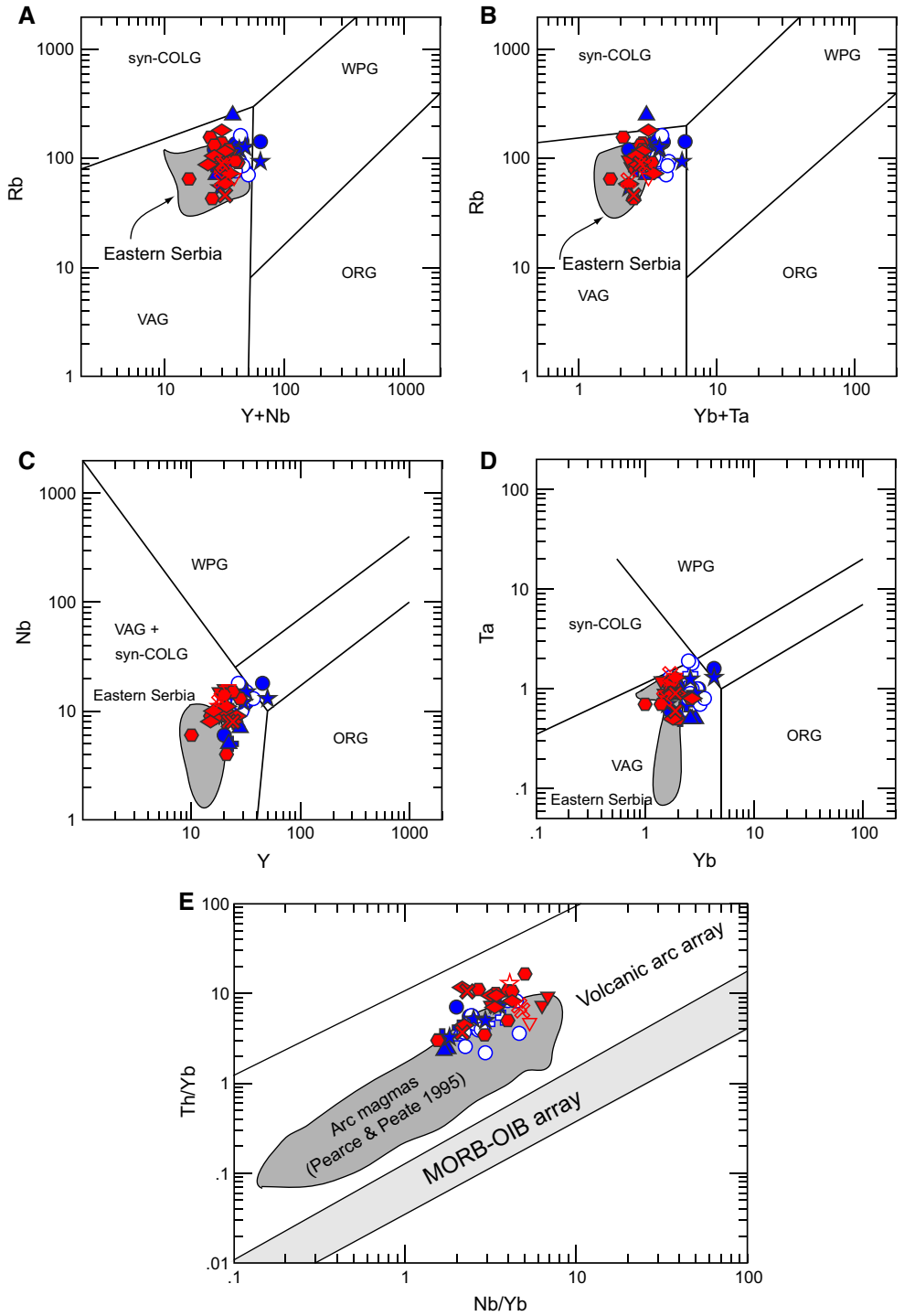

Fig. 9 **a–d** Discrimination diagrams (Pearce et al. 1984) of the Late Cretaceous igneous rocks of the Apuseni Mts. and Banat (Dupont et al. 2002). Data for Eastern Serbia (Kolb et al. 2013) are shown as *grey fields*. **e** Th/Yb versus Nb/Yb diagram of Pearce and Peate (1995) for the Apuseni and Banat (Dupont et al. 2002) samples. Same *symbols* as in Fig. 4

regression line (Fig. 12a, c). When Ba, Zr, Sr are not considered (Fig. 12b) in the first set of samples (R34, R39, R50), the regression line has a plausible slope of 0.65, but the value of the intercept is too low (−3.6) (Fig. 12b). Removing Zn, V, Rb from the regression still gives a too high intercept of −1.6. The intercept can be improved if additional elements such as La, Ce and Nd are also excluded (slope = 0.43, intercept = −0.8). For the second set of sample (R30, R39,

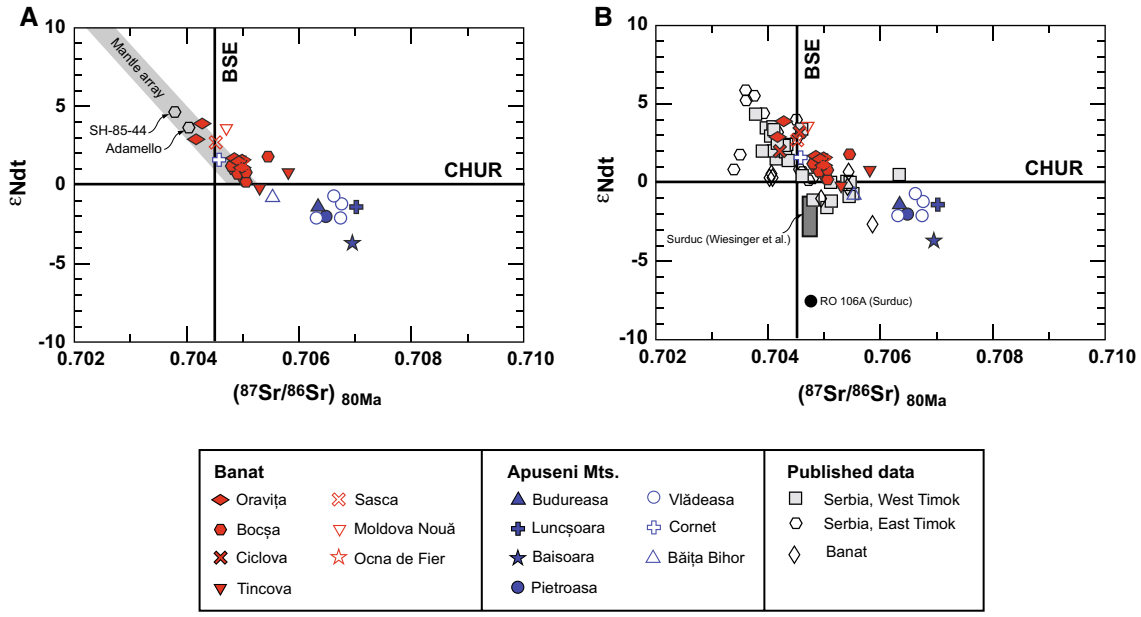

Fig. 10 Initial Sr, Nd isotopic compositions of the Apuseni and Banat (Dupont et al. 2002) samples (**a**). Isotopic compositions have been recalculated back to an 80 Ma age. Sr and Nd isotopic data from Dupont et al. (2002) and this study. Evolution of bulk silicate Earth (BSE) is calculated back from present ratios of $^{87}Sr/^{86}Sr = 0.7047$ and $^{87}Rb/^{86}Sr = 0.0850$ (Faure 1986). Data of Kolb et al. (2013) for Serbia and of Wiesinger et al. (2007) for Banat are shown for comparison (**b**). Mantle array is from De Paolo and Wasserburg (1976)

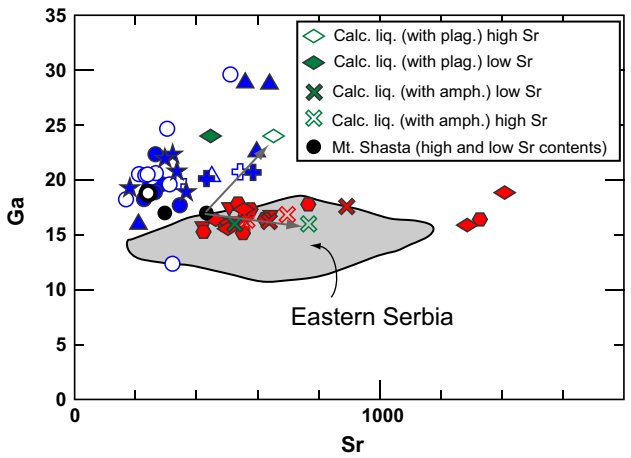

Fig. 11 Ga versus Sr for the Apuseni and Banat (Dupont et al. 2002) samples. Same *symbols* as in Fig. 4. Data for Serbia are from Kolb et al. (2013). The composition of Ga and Sr of sample SH 85-44 of Mt. Shasta (Baker et al. 1994) and of the calculated liquids (amphibole- or plagioclase-bearing cumulates) is also shown for comparison (see text for explanation)

R44), removing Ba, Sr, Zr as well as Zn, V, Rb gives a slope of 0.6 similar to the one obtained for the first set of samples with an intercept close to zero (−0.3) (Fig. 12d). The mixing model could thus explain the differentiation trend if a series of elements are not considered. Tests have been made with other samples selected as the intermediate facies, but Zr, Sr, Ba and sometimes Zn and Rb are outside the regression line. In the Zr–SiO_2 diagram (Fig. 6), data display some dispersion that is probably the cause of the poor correlation obtained for this element in the mixing test. However, Rb, Zn and Sr display good differentiation trends with a good alignment of samples R30, R39 and R44 in these variations diagrams. The negative test of the mixing process is thus not due to samples having their composition affected by mineral accumulation. We thus conclude that magma mixing cannot be fully excluded, but it was not a major process during the differentiation of the Late Cretaceous Apuseni magmas.

Fractional crystallization and batch partial melting can be discriminated in a log C_A –log C_B diagram using the most compatible element (A) versus the most incompatible element (B) (Joron et al. 1978; Martin 1987). Indeed, the slope of the trend is $\frac{D_B(1-D_A)}{D_A(1-D_B)}$ and $\frac{D_A-1}{D_B-1}$ for a partial melting and a fractional crystallization process, respectively. As D_A and D_B are significantly higher and lower than 1, respectively, the slope of the trend can be simplified and will be close to $-D_A$ for a fractional crystallization process and $-D_B$ for a partial melting process. Among trace elements, Th appears as strongly incompatible and Zn, as strongly compatible. For the Vlădeasa and Budureasa samples, the slope of the trend in a $\log_{Zn}$–$\log_{Th}$ diagram is −1.1. A fractional crystallization process thus better predicts the differentiation trend.

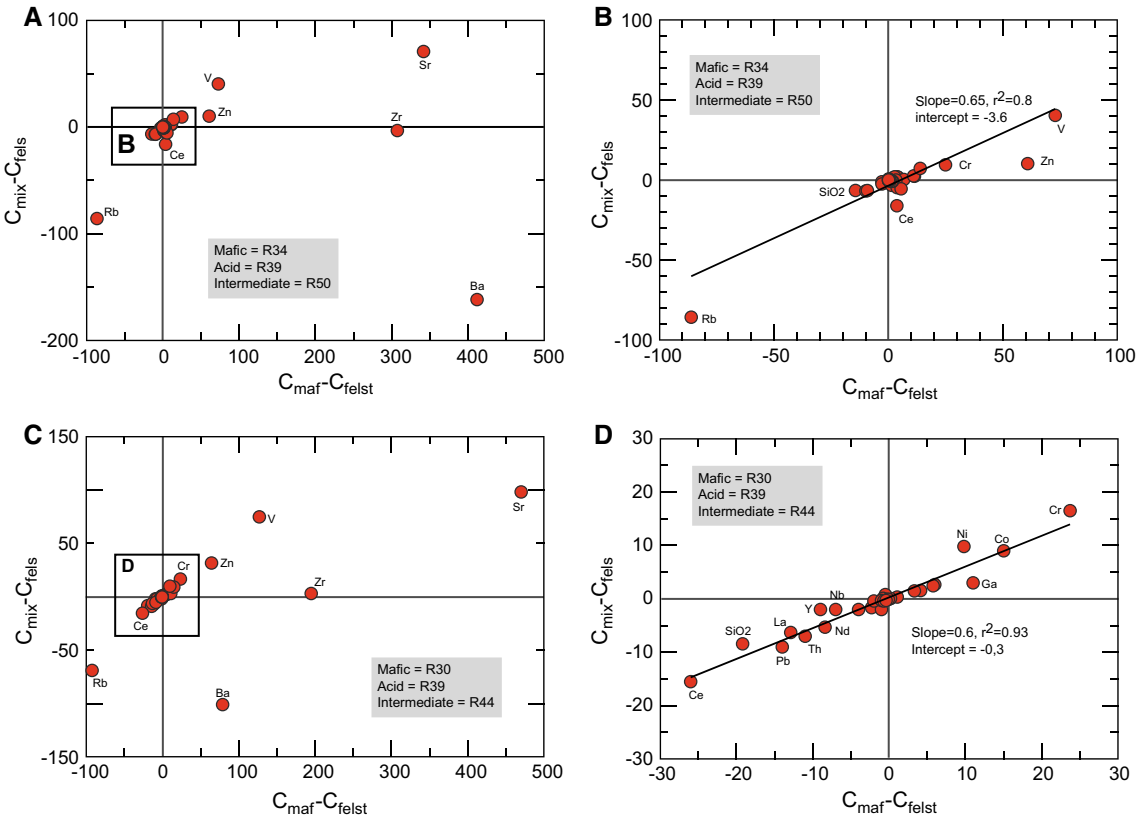

Fig. 12 Test of a mixing process according to Fourcade and Allègre (1981). C_{maf}, C_{fels} and C_{mix} are the concentrations in the mafic, felsic and mixed facies. The hypothetical proportion (X) of the mafic component in the mixing process is given by the slope of the regression line. See text for explanation

Modelling of the fractional crystallization process

The fractional crystallization process has been modelled with the least square regression method in three steps that are summarized in Table 4. In the first step, subtraction of a gabbronoritic cumulate drives the liquid from 53.64 % SiO_2 to 56.95 SiO_2 leaving 73 % of residual liquid at this stage. Further differentiation to a proportion of 36 % of residual liquid (64.73 % SiO_2) is produced by subtraction of a dioritic cumulate containing apatite. The most evolved composition (72.43 % SiO_2) is finally reached when the proportion of residual liquid is 21 %. The third cumulate is also dioritic but with a more albitic plagioclase.

The composition of the cumulates derived with the least square regression method on major elements can be tested using the trace element composition and the Rayleigh distillation law:

$$C_L = C_0 . F^{(D-1)}$$

where C_0 and C_L are the concentrations of the trace element in, respectively, the starting composition and the residual liquid, F is the fraction of residual liquid that has been calculated with the least square regression method and D, the bulk partition coefficient, equals $\Sigma D_i.X_i$. D_i is the partition coefficient of the trace element between mineral i and the liquid, and X_i is the proportion of this mineral in the subtracted cumulate. X_i has also been calculated with the least square regression method.

Partition coefficients were selected from the literature for andesitic to dacitic compositions and are given in Table 5. In the first step of differentiation, the calculated composition of the residual liquid compares rather well with the composition of sample R27 except for Ba and Zn (Table 6). Ba is lower in the calculated liquid (781 ppm) than in R27 (1514 ppm). However, sample R27 as well as samples R29 and R34 have a Ba content significantly higher than the main trend suggesting some mineral accumulation. The calculated Ba content is within the range observed in the samples having a SiO_2 content close to that of R27 (referred to L1 samples below and as "Range L1" in Table 6). The calculated Zn content in L1 (93 ppm) is higher than the Zn content of sample R27 (64 ppm) but hereto in the range of L1 samples. In the second step, the composition of

Table 4 Results of least-squares modeling calculations for major elements

	STEP1		STEP2		STEP3	
	L0 = R30	L1 = R27	L0 = R27	L1 = R44	L0 = R44	L1 = R39
SiO_2	53.64	56.95	56.95	64.73	64.73	72.43
TiO_2	1.52	1.20	1.20	0.76	0.76	0.42
Al_2O_3	18.72	19.25	19.25	16.07	16.07	14.27
FeOt	8.45	6.46	6.46	5.03	5.03	2.26
MnO	0.19	0.10	0.10	0.10	0.10	0.06
MgO	4.12	2.75	2.75	2.23	2.23	0.70
CaO	7.84	6.20	6.20	4.41	4.41	1.87
Na_2O	3.37	4.22	4.22	3.96	3.96	3.71
K_2O	1.86	2.40	2.40	2.53	2.53	4.17
P_2O_5	0.29	0.47	0.47	0.18	0.18	0.11
	100.00	100.00	100.00	100.00	100.00	100.00
Composition of calculated daughter liquids (observed composition-calculated composition)						
SiO_2	56.94 (0.01)		64.72 (0.01)		72.45 (−0.02)	
TiO_2	1.20 (0.00)		0.76 (0.00)		0.42 (0.00)	
Al_2O_3	19.26 (−0.01)		16.11 (−0.04)		14.47 (−0.20)	
FeOt	6.46 (0.00)		5.03 (0.00)		2.25 (0.01)	
MnO	0.16 (−0.06)		0.09 (0.01)		0.05 (0.01)	
MgO	2.78 (−0.03)		2.36 (−0.13)		0.73 (−0.03)	
CaO	6.21 (−0.01)		4.25 (0.16)		1.77 (0.10)	
Na_2O	4.25 (−0.03)		4.12 (−0.16)		3.02 (0.69)	
K_2O	2.54 (−0.14)		2.35 (0.18)		3.85 (0.32)	
P_2O_5	0.40 (0.07)		0.39 (−0.21)		0.23 (−0.12)	
Phase composition and proportions (%) and in the subtracted cumulate						
Plagioclase	An83	50.4	An46	70.8	An33	63.3
Ca-poor px	Mg# 62	25.1				
Ca-rich px	Mg# 75	15.5				
Amphibole			Mg# 60	4.5	Mg# 60	31.8
Biotite			Mg# 54	19.5	Mg# 54	0.2
Magnetite	Mt64Usp36	5.9	Mt64Usp36	3.7	Mt64Usp36	4.3
Ilmenite	Ilm87Hm13	3.2	Ilm87Hm13	0.2	Ilm87Hm13	0.1
Apatite				1.3		0.3
Σr^2		0.017		0.034		0.228
F (proportion residual liquid)		0.73		0.36		0.21

sample R27 has been considered as the starting composition except for Ba, Co and Zn. For these three elements, the starting content has been interpolated from the main differentiation trend displayed by the Budureasa and Vlădeasa samples. The calculated composition is very close to that of sample R44 (Rb, REE, V, Co, Zn) or in the range of the L1 samples (Sr, Ba). Similarly, in the third step, the calculated composition is very close to the trace element content of sample R39 (Sr, Ba, REE, V, Zn) or close to the L1 samples (Rb, Co). The trace element contents thus support the mineral proportions of the three cumulates derived from the least square regression method.

The parent magmas of the Apuseni and Banat Late Cretaceous igneous rocks

Because the Late Cretaceous igneous rocks from Banat and the Apuseni Mts. crosscut the Mid-Cretaceous nappe piles and are extruding in Gosau-type basins, we consider that they were emplaced during the post-collisional stage of the belt. Their high-K calc-alkaline character, that is typical of this geodynamic setting (Liégeois et al. 1998), supports this conclusion. Harris et al. (1986) pointed out that post-collisional and arc magmas are difficult to discriminate geochemically and further suggested that the mantle component of the post-collisional magmas is produced from a

Table 5 Partition coefficients for trace elements

	STEP1					STEPS 2 and 3					
	plag	opx	cpx	mgt	ilm	plag	amph	bio	apatite	mgt	ilm
Rb	0.3[a]	0.062[b]	0.03[a]	0.01[a]	0.01[a]	0.3[a]	0.18[b]	1.35[g]	0.01[a]	0.01[a]	0.01[a]
Sr	2.3[r]	0.068[b]	0.5[a]	0.01[a]	0.01[a]	4[r]	0.01[a]	0.31[a]	2[a]	0.01[a]	0.01[a]
Ba	1.8[a]	0.07[b]	0.1[a]	0.1[a]	0.01[a]	0.17[l]	0.62[e]	6.36[q]	0.01[a]	0.1[a]	0.01[a]
Ce	0.2[a]	0.082[c]	0.075[d]	0.71[a]	0.0019[k]	0.2[a]	0.53[a]	0.32[a]	21.1[i]	0.71[a]	0.0019[k]
Sm	0.1[a]	0.133[c]	0.22[d]	1.2[a]	0.0023[k]	0.1[a]	2[a]	0.26[a]	46[i]	1.2[a]	0.0023[k]
Eu	2[a]	0.113[c]	0.2[d]	0.91[a]	0.0009[k]	2[a]	1.9[a]	0.24[a]	25.5[i]	0.91[a]	0.0009[k]
Tb	*0.1*[a]	0.215[c]	0.258[d]	1.3[a]	0.0095[k]	*0.1*[a]	2[a]	0.28[a]	39.4[i]	1.3[a]	0.0095[k]
Yb	0.1[a]	0.73[c]	0.3[d]	0.44[a]	0.057[k]	0.1[a]	2.1[a]	0.44[a]	15.4[i]	0.44[a]	0.057[k]
V	0.2[a]	1.2[l]	12[l]	1.2[j]	14[j]	0.2[a]	4.92*[,f]–17**[,f]	0.0001	0[a]	1.2[j]	14[j]
Co	0.1[a]	3.4[l]	2.4[l]	5[o]	11[j]	0.1[a]	6.1[a]	4[g]	0.01[a]	5[o]	11[j]
Zn	0.17[b]	2.6[m]	0.3[n]	2.6[p]	8.3[b]	0.17[b]	1.6*[,a]–8**[,b]	11.4[h]	0.01[a]	2.6[p]	8.3[b]

Plag plagioclase, *opx* orthopyroxene, *cpx* clinopyroxene, *mgt* magnetite, *ilm* ilmenite, *amph* amphibole, *bio* biotite

* Partition coefficient used in step 2; ** partition coefficient used in step3

[a] Bacon and Druitt (1988), [b] Ewart and Griffin (1994), [c] Nagasawa and Schnetzler (1971), [d] McKay (1989), [e] Nagasawa (1973), [f] Sisson (1994), [g] Villemant (1988), [h] Bea et al (1994), [i] Fujimaki (1986), [j] Toplis and Corgne (2002), [k] Nakamura et al (1986), [l] Ewart et al.(1973), [m] Luhr and Carmicahel (1980), [n] Dostal et al (1983), [o] Horn et al (1994), [p] Esperança et al. (1997), [q] Philpotts and Schnetzler (1970), [r] Duchesne (1978)

source above a subduction zone, i.e. a mantle wedge that has been enriched in LILE. In the following, we will thus discuss the petrology of the Late Cretaceous igneous rocks using experimental and geochemical data obtained on arc magmas.

As the least differentiated samples from the Apuseni Mts. and Banat have a low Mg# (below 0.5 in the Apuseni and below 0.55 in Banat) as well as Cr and Ni contents below 55 ppm and 25 ppm, respectively, these samples cannot be representative of primary magmas in equilibrium with a mantle source as these magmas are inferred to have an Mg# > 0.7 and high Cr and Ni contents (e.g. Grove et al. 2012). Compared to sample SH-85-44C, recognized as a near-primary magma of Mont Shasta (Cascade Range, USA) (Grove et al. 2012), the least differentiated compositions of the Banat and Apuseni Mts. trends are indeed significantly lower in MgO (Fig. 5). Consequently, the least differentiated samples, parent magmas of the Apuseni and Banat differentiation trends, were either produced by partial melting of a lower crustal source or are the result of lower crustal differentiation from a precursor mantle melt as interpreted for the Late Cretaceous magmatism from Serbia (Kolb et al. 2013) and for the Tertiary Alpine intrusions such as Bergell (von Blanckenburg et al. 1992, 1998) and Adamello (Ulmer et al. 1983; Macera et al. 1983; Kagami et al. 1991). Partial melting of a lower crustal source to produce mafic magmas would require extensive melting of an ultramafic source at very high temperature. This process seems unlikely as there is no evidence of an important thermal anomaly associated with the Late Cretaceous magmatism. We thus retain the second hypothesis, lower crustal differentiation from a mantle-derived melt. Moreover, as the parent magmas of the Banat and Apuseni Mts. differentiation trends have overlapping major and trace element composition, except for Ga and Sr (see discussion in the next section), we consider that they were derived from the same mantle melt.

Lower crustal differentiation of the mantle-derived melt and the question of Ga and Sr

It has already been pointed out that in a Ga–Sr diagram (Fig. 11), the Apuseni Mts. magmatic rocks display a significantly higher Ga content and a slightly lower Sr content than the Banat magmatic rocks. This also holds for the least differentiated samples (parent magmas) of the two trends. These differences could result either from precursor mantle melts with different Sr and Ga contents or from the differentiation processes that produced the parent magmas of both trends from the mantle melts.

In a subduction-related geodynamic setting, the composition of primary magmas reflects contributions from the slab (including subducted sediment: Plank and Langmuir 1993) and the overlying mantle wedge (e.g. Gill 1981; Plank and Langmuir 1993). These magmas are enriched in LILE (Rb, Cs, Th, Pb) relative to the HFSE (Nb, Ta, Zr, Hf, TiO_2) that display negative anomalies compared to primary MORBs or OIBs, and these geochemical patterns are considered as resulting from the slab contribution (e.g. Gill 1981; Plank and Langmuir 1993). In a Th/Yb versus Nb/Yb diagram, arc magmas have thus notably higher Th/Yb ratios than the MORB

Table 6 Results of trace elements modelling

	STEP1 L0 = R30	L1 = R27	Range L1**	Calculated L1
Rb	71	74	74–94	91
Sr	639	597	322–597	592
Ba	768	1514	448–2470	781
Ce	40	56	49.5–69.4	51
Sm	4.6	5.4	5.0–7.1	5.9
Eu	1.9	2.2	1.5–2.4	1.8
Tb	0.6	0.7	0.6–1.0	0.8
Yb	2.6	2.7	2.1–3.2	3.2
V	160	93	65–206	94
Co	22	12	12–32	17
Zn	99	64	59–96	93
	STEP2 L0 = R27	L1 = R44	Range L1**	Calculated L1
Rb	74	94	77–143	85.8
Sr	597	267	240–367	343.6
Ba	*700**	588	527–723	625.0
Ce	55.7	50.2	46.8–78.8	63.7
Sm	5.4	5.2	3.8–8.3	5.6
Tb	0.7	0.8	0.6–1.3	0.8
Eu	2.2	1.3	0.9–1.9	1.7
Yb	2.7	2.7	1.8–4.3	3.2
V	93.0	107.7	47.7–107.7	109.4
Co	*17**	16	8–16	15.0
Zn	*93**	66.4	53.2–66	60.0
	STEP3 L0 = R44	L1 = R39	Range L1**	Calculated L1
Rb	94	163	121–250	117
Sr	267	169	169–210	171
Ba	588	689	647–689	715
Ce	50.2	65.7	61.2–65.7	60
Sm	5.2	5.2	4.0–5.2	5
Eu	1.3	1.3	0.8–1.3	1
Tb	0.8	0.8	0.6–0.8	1
Yb	2.7	3.0	2.0–3.0	3
V	107.7	33.0	32.2–47.8	29
Co	16	7	3–10	11
Zn	66.4	34.9	34.9–72.4	34

* Derived from the differentiation trend. See text for explanation

** Range of composition displayed by the samples having a SiO_2 content close to that of sample R27, R44, R39, respectively

array (Pearce 1983; Pearce and Peate 1995) (Fig. 9e). Ga and Sr have different geochemical behaviours: Ga is not contributed from the slab (in a Ga/Yb versus Nb/Yb diagram arc magmas plot in the MORB array), whereas Sr is (Pearce and Peate 1995). Consequently, variable trace element content of the mantle source would not produce high Ga and low Sr contents (Apuseni parent magma) versus low Ga and high Sr contents (Banat parent magma). Moreover, we note that in the Th/Yb versus Nb/Yb diagram (Fig. 9e), the Apuseni Mts. and Banat samples overlap in composition suggesting similar contribution of LILE from the slab.

We have tested the hypothesis that the different Ga and Sr contents were produced during the lower crustal differentiation of a mantle-derived magma using the experimental data of Müntener et al. (2001) performed at 1.2 GPa on sample SH-85-44, a near-primary magma composition at Mont Shasta. These experimental data indicate that when the H_2O content of the melt is above 3 wt%, amphibole crystallizes early and the liquidus temperature of plagioclase is lowered. More particularly, when their starting composition has an H_2O content of 5 wt% (run B704 of Müntener et al. (2001)), the cumulate contains amphibole (45 %), orthopyroxene (19 %), clinopyroxene (36 %) and trace amount of garnet, whereas in their run B668 with a lower H_2O content (2.5 wt% in the starting composition), the melt is in equilibrium with a cumulate made of plagioclase (27 %), orthopyroxene (34 %) and clinopyroxene (39 %). The experimental melts of runs B704 (with amphibole) and B668 (with plagioclase) have a major element composition very close to that of samples 98R12 (Dupont et al. 2002) and R30, parent magmas of the Banat and Apuseni differentiation trends, respectively (Fig. 5) supporting the hypothesis that these mafic magmas were derived by differentiation from a precursor mantle melt. Using appropriate partition coefficients (amphibole: 1.77 (Ewart and Griffin 1994), orthopyroxene: 0.32 (Ewart and Griffin 1994), clinopyroxene: 0.69 (Blundy et al. 1998), plagioclase: 0.08 (Blundy et al. 1998)), a Ga content of 17 ppm for the primary magma (sample 85-44 of Mount Shasta: Baker et al. 1994) and the Rayleigh distillation law, the Ga content of the residual melt is 24 ppm and 16 ppm when subtracting the plagioclase-bearing and amphibole-bearing cumulates, respectively. This agrees very well with the observed Ga contents of samples R30 (29 ppm) (parent magma of the Apuseni trend) and 98R12 (16.2 ppm) (parent magma of the Banat trend). Similarly, using the Sr content of sample 85-44 (295 ppm: Baker et al. 1994), the calculated Sr content of the residual melt is higher when subtracting the amphibole-bearing cumulate (524 ppm) than the plagioclase-bearing cumulate (445 ppm). The calculated values are lower than the observed Sr contents [766 ppm in sample 98R12 (Banat); 639 ppm in sample R30 (Apuseni)], but precise constraints on the Sr content of the mantle-derived magma are not available and subduction-related primary magmas have rather variable Sr contents (41 up to 745 ppm: Grove et al. (2012) and references therein). When considering 431 ppm Sr in the primary mantle melt, in the range of the Sr content of primary magmas, the calculated Sr content of the residual liquid is 766 ppm and 651 ppm with the amphibole- and plagioclase-bearing cumulates, respectively. The slightly higher TiO_2 content of the Apuseni differentiation trend (Fig. 5) compared to the Banat trends can also be predicted with these two different cumulates as amphibole has a higher TiO_2 content than plagioclase. It is thus plausible that the different Ga and Sr contents in the parent magmas of both trends (Banat versus Apuseni) are due to a different H_2O content of the mantle-derived magma. A higher H_2O content in the primary magma of Banat induces early crystallization of amphibole, thus decreasing the Ga content and increasing the Sr content in the derivative liquids, whereas a lower H_2O content in the Apuseni induces early crystallization of plagioclase, thus decreasing the Sr content and increasing the Ga content in the derivative liquids. Interestingly, the Late Cretaceous magmatic rocks from Serbia (Timok, Ridajn-Krepolijn), for which amphibole was also considered as a high- and/or low-pressure fractionating phase (Kolb et al. 2013), display similar Sr, Ga and TiO_2 contents than the Banat trend (Fig. 11).

Crustal contamination

As mentioned above, samples from the Apuseni Mts. and Banat have different isotopic compositions except that the sample of Cornet (Apuseni Mts.) plots in the field of samples from Banat (Fig. 10), maybe because, before its final emplacement in calcareous marbles, this latter intrusion has crosscut the formations of the Mureş zone (Fig. 2) that are essentially made of Jurassic mafic rocks of MORB affinity overlain by calc-alkaline lavas (Bortolotti et al. 2002). The sample from Băiţa Bihor is also close to the Banat field. Most Banat samples plot on the mantle array and two of them (Oraviţa) are also close to the composition of near-primary arc magmas from North America (Mt-Shasta: Grove et al. 2002) and Adamello (Kagami et al. 1991). The rest of the Romanian banatite samples are displaced towards higher initial Sr isotopic composition and lower epsilon Nd (Apuseni Mts.) compared to the mantle array. Instead of displaying a continuous trend of decreasing epsilon Nd and increasing Sr_i, the Late Cretaceous igneous rocks of Romania more or less define three discrete groups (Fig. 10). One group plots close to the composition of primary arc magmas. A second group, comprising most of Banat samples has mildly positive epsilon Nd and clusters around an Sr_i of 0.705. The third group includes most of the Apuseni samples and displays negative epsilon Nd and high Sr_i. This split in three groups is in agreement with the lack of correlation with wt% SiO_2. The first group likely witnesses the isotopic composition of the mantle source. The other two groups probably evidence crustal contamination. As the Banat and Apuseni Mts. igneous rocks were emplaced in two different crustal segments, respectively, the Dacia and Tisza blocks, the occurrence of distinct isotopic composition probably results from the interaction with two different crustal contaminants. The Sr and Nd isotopic compositions of the geological formations that make the Tisza and

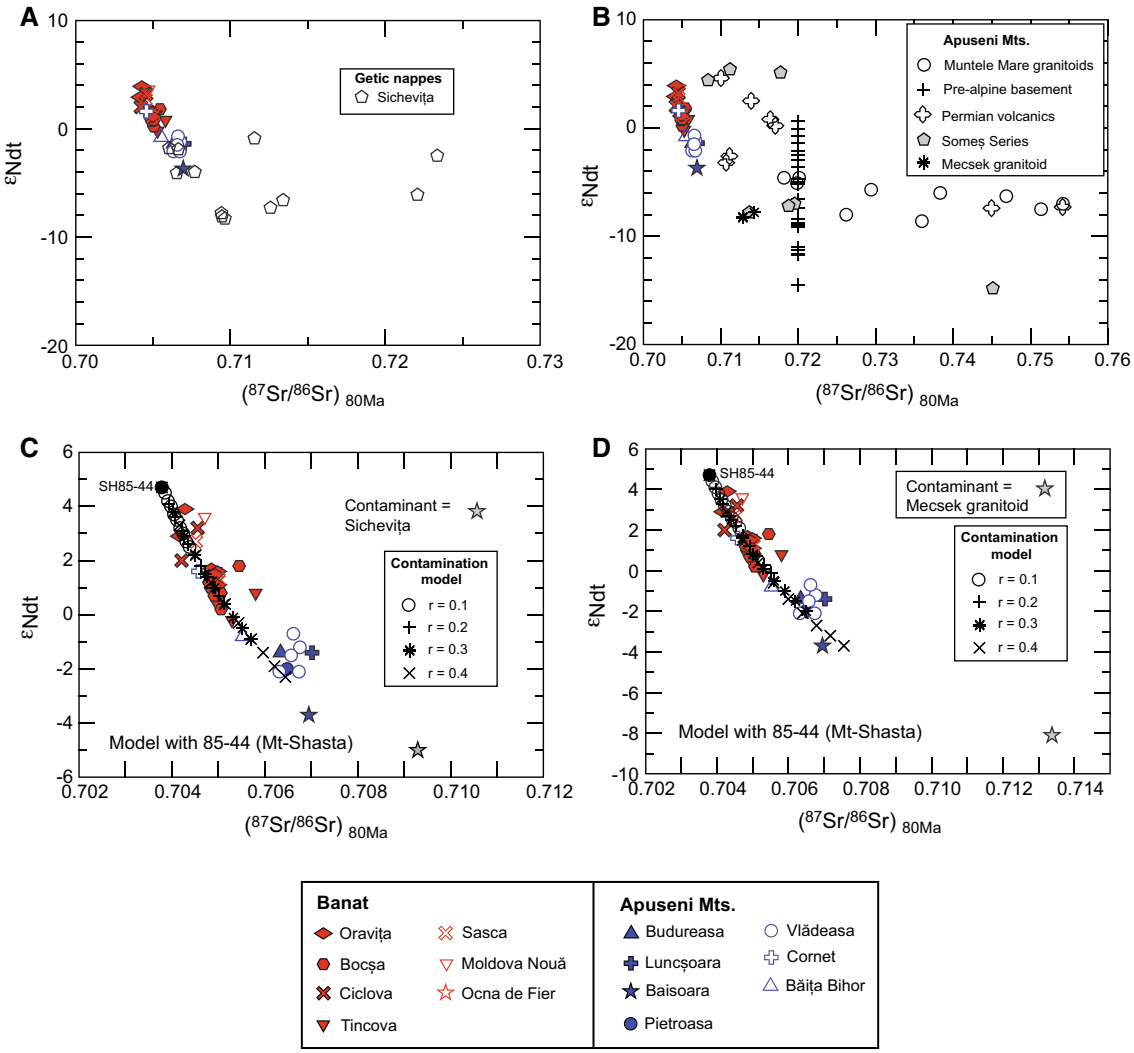

Fig. 13 Epsilon Nd_t versus initial Sr isotopic compositions of the Apuseni and Banat (Dupont et al. 2002) samples compared with possible contaminants of the Getic nappes (**a**) (Duchesne et al. 1997, 2008) and of the Apuseni Mountains [Permian volcanics (Nicolae et al. 2014); Muntele Mare granitoid and surrounding rocks (Somes Series) (Anton 2000; Balintoni et al. 2014; Balintoni, pers comm); granito-gneisses from the Apuseni Mts. (Pană et al. 2002)] and the Mecsek granitoid from the Tisza block in Hungary (Klötzli et al. 2004) (**b**). AFC model (De Paolo 1981; Ersoy and Helvaci 2010) using the Sr and Nd isotopic composition as well as the Sr and Nd content (Grove et al. 2002) of sample 85-44 (Mt-Shasta) as the starting composition and, as the contaminant, the average Sr and Nd isotopic composition of the Sichevița (Duchesne et al. 2008) (**c**), or the Mecsek granite (Klötzli et al. 2004) (**d**)

Dacia blocks have not been extensively studied, but data are available for the granitoids belonging to the basement of the Getic nappes in the South Carpathians (Duchesne et al. 1997, 2008) (Dacia block) (Fig. 13a), the pre-Alpine crust in the Apuseni Mountains (Fig. 13b) [northern and southern terranes as well as the Highis–Biharia zone; Permian volcanics (Nicolae et al. 2014); Muntele Mare granitoid and surrounding rocks (Somes Series) (Anton 2000; Balintoni et al. 2014; Balintoni, pers comm) and the Variscan Mecsek granitoid from the Tisza block in Hungary (Klötzli et al. 2004)]. Available isotopic data show rather overlapping composition in the two blocks with, however, higher Sr_i and more negative epsilon Nd in the Tisza block, especially for the granito-gneisses analysed by Pană et al. (2002) for which no Sr isotopic composition is given. Crustal contamination has been tested with an AFC model as described by De Paolo (1981) and Ersoy and Helvaci (2010). As in the epsilon Nd_t versus Sr_i, the Romanian samples seem to cluster in three discrete groups, and within each of these groups, the isotopic composition (Sr_i, epsilon Nd) is not correlated with the SiO_2 content, and we suggest that assimilation occurred very early, probably when the primary mantle-derived magma differentiated towards the composition of the parent magmas of the Apuseni and Banat trends. We used the average isotopic composition of the Mecsek (Klötzli et al. 2004) and

Sicheviţa (Duchesne et al. 2008) granitoids (Fig. 13c, d) as possible contaminants of the Apuseni and Banat magmatic rocks, respectively. The Sicheviţa intrusion indeed belongs to the Getic nappes that have been crosscut by the Late Cretaceous magmas. The Sr and Nd contents of the bulk continental crust (Sr = 320 ppm; Nd = 20 ppm) (Rudnick and Gao 2003) were selected for the element composition of the contaminants, and the experimental amphibole- (Fig. 13c) and plagioclase-bearing (Fig. 13d) cumulates of Müntener et al. (2001) were used to model the fractional crystallization process. Results are displayed in Fig. 13c, d and show that with an *r* value (fraction of crust assimilated versus crystals formed) of 0.3–0.4, it is possible to predict the isotopic composition of the Banat and Apuseni magmatic rocks, thus supporting the hypothesis of two distinct contaminants.

Conclusions

The geochemical and isotopic data presented here provide constraints on the petrology of the Late Cretaceous igneous rocks of Romania and lead to the following conclusions:

1. The parent magma of the Apuseni Mountains Late Cretaceous magmatism is a basaltic andesite that differentiated to rhyolitic composition mainly by a fractional crystallization process. The Al-in hornblende geobarometer indicates that this process occurred in upper crustal storage chambers.
2. Because of their too low Mg#, the parent magmas of the Apuseni and Banat differentiation trends cannot be considered as primary magmas. The experimental data acquired by Müntener et al. (2001) on a primary magma at 1.2 GPa indicate that they could have been produced by lower crustal fractionation from a primary mantle melt.
3. The Apuseni and Banat magmatic rocks display overlapping differentiation trends in variation diagrams except for Ga and to a lesser extent Sr. The parent magma of the Apuseni trend has a higher Ga and slightly lower Sr content than the parent magma of the Banat trend. This difference can be taken into account by a higher H_2O content in the Banat mantle-derived magma which induces early crystallization of amphibole at the expense of plagioclase. Amphibole has indeed a high and low partition coefficient for Ga and Sr, respectively. As the Timok and Ridanj-Krepolijn Late Cretaceous magmatic rocks (Kolb et al. 2013) overlap with the Banat samples in the Ga–Sr diagram, this suggests that the H_2O content of the mantle-derived magmas varied along the belt.
4. The Banat and Apuseni samples have contrasting isotopic compositions that can be taken into account by contamination with two different contaminants in agreement with the emplacement of the Banat and Apuseni magmatic rocks in two different crustal terranes, respectively, Dacia and Tisza.

Acknowledgments This work was supported by grants from the CGRI of Belgium to J. Vander Auwera and by FNRS Grants 2.4530.98 and 2.4512.00. It is partly based on the work carried out by J. Gesels during her Master's degree. The authors would like to thank C. Pin (Université Blaise Pascal, Clermont-Ferrand) for his contribution during the radiogenic isotopes analyses. Careful reviews by N. Bonev and P. Barbey improved the manuscript.

References

Andrei J, Cristescu T, Calota C, Proca A, Romanescu D, Russo-Săndulescu D, Ştefan A, Suceavă M, Bradu M, Hannich D, Albaiu M (1989) Spatial distribution and structural images of banatites from Romania deduced from gravity and magnetic data. Rev Roum Géol Géophys Géogr Sér Géophys 33:79–85

Anton D (2000) Petrographical, geochemical and isotopic study of Mt. Mare granitoids, North Apuseni Mountains. Evolution of peraluminous magma. PhD Thesis, Cluj-Napoca, 176 pp

Antonijević I, Grubić A, Đjorđević M (1974) The upper Creaceous paleorift in Eastern Serbia. In: Metallogeny and concepts of the geotectonic development of Yugoslavia. Belgrade University, Belgrade

Bacon CR, Druitt TH (1988) Compositional evolution of the zoned calc-alkaline magma chamber of Mount Mazama, Crater Lake, Oregon. Contrib Mineral Petrol 98:224–256

Baker M, Grove T, Price R (1994) Primitive basalts and andesites from the Mt. Shasta region, N. California: products of varying melt fraction and water content. Contrib Mineral Petrol 118:111–129

Balintoni I, Balica C, Cliveți M, Li LQ, Hann H, Chen F, Schuller V (2009) The emplacement age of the Muntele mare Variscan granite (Apuseni Mountains, Romania). Geol Carpath 60(6):495–504

Balintoni I, Balica C, Ducea M, Hann H-P (2014) Peri-Gondwanan terranes in the Romanian Carpathians: a review of their spatial distribution, origin, provenance, and evolution. Geosci Front 5:395–411

Bea F, Pereira M, Stroh A (1994) Mineral/leucosome trace-element partitioning in a peraluminous migmatite (a laser ablation-ICP-MS study). Chem Geol 117:291–312

Berza T, Ilinca G (2014) Late Cretaceous Banatitic magmatism and metallogeny in the frame of the Eoalpine tectonics from the Carpathian–Balkan orogen. In: Beqiraj A. et al (ed) XXth congress of the Carpathian–Balkan geological association. Buletini i Shkencave Gjeologjike, Tirana (Albania), pp 145–148

Berza T, Constantinescu E, Vlad S-N (1998) Upper Cretaceous magmatic series and associated mineralisation in the Carpathian–Balkan Orogen. Resour Geol 48(4):291–306

Bleahu M, Soroiu M, Catilina R (1984) On the Cretaceous tectonomagmatic evolution of the Apuseni Mountains as revealed by K–Ar dating. Rev Roum Phys 29:123–130

Blundy J, Robinson J, Wood B (1998) Heavy REE are compatible in clinopyroxene on the spinel lherzolite solidus. Earth Planet Sci Lett 160:493–504

Bogaerts M (1998) Etude pétrographique et géochimique des dykes autour des intrusions de Biella et de Traversella (Alpes

Nord-Occidentales, Italie). Master Thesis, University of Liège, Liège, 65 pp
Bogaerts M, Vander Auwera J (1999) Potassic and ultrapotassic dikes around the plutons of Biella and Traversella. In: Fourth Hutton symposium on the origin of granites and related rocks (Clermont-Ferrand, France), vol 290, p 46
Bortolotti V, Marroni M, Nicolae I, Pandolfi L, Principi G, Saccani E (2002) Geodynamic implications of jurassic ophiolites associated with Island-Arc volcanics, South Apuseni Mountains, Western Romania. Int Geol Rev 44(10):938–955
Csontos L, Vörös A (2004) Mesozoic plate tectonic reconstruction of the Carpathian region. Paleogeogr Paleoclimatol Paleoecol 210:1–56
Dal Piaz G, Venturelli G, Scolari A (1979) Calc-alkaline to ultrapotassic postcollisional volcanic activity in the internal northwestern Alps. Mem Sci Geol 32:4–15
De Paolo DJ (1981) Trace-element and isotopic effects of combined wallrock assimilation and fractional crystallization. Earth Planet Sci Lett 53:189–202
De Paolo DJ, Wasserburg G (1976) Inferences about magma sources and mantle structure from variations of 143Nd/144Nd. Geophys Res Lett 3:743–746
Defant M, Kepezhinskas P (2001) Adakites: a review of slab melting over the past decade and the case for a slab-melt component in arcs. EOS Trans Am Geophys Union 82:68–69
Dostal J, Dupuy C, Carron JP, Dekerneizon ML, Maury RC (1983) Partition coefficients of trace elements-application to volcanic rocks of St-Vincent, West-Indies. Geochim Cosmochim Acta 47(3):525–533
Duchesne JC (1978) Quantitative modeling of Sr, Ca, Rb and K in the Bjerkrem-Sogndal layered lopolith (S.W. Norway). Contrib Mineral Petrol 66:175–184
Duchesne JC, Berza T, Liégeois J-P, Vander Auwera J, Demaiffe D, Andar P, Tatu M, Teleman C, Stan N, Iancu V (1997) Geochemistry of Romanian granites, University of Liège, CIPA-CT93-0237, p 158
Duchesne JC, Liégeois J-P, Iancu V, Berza T, Matukov DI, Tatu M, Sergeev SA (2008) Post-collisional melting of crustal sources: constraints from geochronology, petrology and Sr, Nd isotope geochemistry of the Variscan Sichevita and Poniasca granitoid plutons (South Carpathians, Romania). Int J Earth Sci 97(4):705–723
Dupont A, Vander Auwera J, Pin C, Marincea S, Berza T (2002) Trace element and isotope (Sr, Nd) geochemistry of porphyry- and skarn-mineralising Late Cretaceous intrusions from Banat, western South Carpathians, Romania. Miner Depos 37(6–7):568–586
Ersoy Y, Helvaci C (2010) FC-AFC-FCA and mixing modeler: a microsoft EXCEL spreadsheet program for modeling geochemical differentiation of magma by crystal fractionation, crustal assimilation and mixing. Comput Geosci 36:383–390
Esperança S, Carlson R, Shirey S, Smith D (1997) Dating crust-mantle separation: Re–Os isotopic study of mafic xenoliths from central Arizona. Geology 25(7):651–654
Ewart A, Griffin W (1994) Application of proton-microprobe data to trace-element partitioning in volcanic rocks. Chem Geol 117:251–284
Ewart A, Bryan W, Gill J (1973) Mineralogy and geochemistry of the Younger Volcanic Islands of Tonga, SW Pacific. J Petrol 14(3):429–465
Faure G (1986) Principles of isotope geology. Wiley, New York
Fourcade S, Allègre CJ (1981) Trace elements behaviour in granite genesis: a case study, the calc-alkaline plutonic association from the Quérigut complex (Pyrénées, France). Contrib Mineral Petrol 76:177–195
Frost BR, Frost CD (2008) A geochemical classification for feldspathic igneous rocks. J Petrol 49(11):1955–1969
Frost BR, Arculus RJ, Barnes CG, Collins WJ, Ellis DJ, Frost CD (2001) A geochemical classification of granitic rock suites. J Petrol 42:2033–2048
Fujimaki H (1986) Partition coefficients of Hf, Zr, and REE between zircon, apatite and liquid. Contrib Mineral Petrol 94(1):42–45
Georgiev S, Von Quadt A, Heinrich C, Peytcheva I, Marchev P (2012) Time evolution of a rifted continental arc: integrated ID-TIMS and LA-ICPMS study of magmatic zircons from the Eastern Srednogorie, Bulgaria. Lithos 154:53–67
Gesels J (2003) Pétrologie et géochimie des banatites des Monts Apuseni (Roumanie). Master thesis Thesis, Liège, 100 pp
Gill J (1981) Orogenic andesites and plate tectonics. Minerals and rocks, Springer, Berlin, Heidelberg 16:392
Giuşcă D, Istrate G, Ştefan A (1969) Le complexe volcano-plutonique de la Vlădeasa (Roumanie). Bull Volcanol XXXIII(4):13–45
Grove T, Parman S, Bowring S, Price R, Baker M (2002) The role of an H2O-rich fluid component in the generation of primitive basaltic andesites and andesites from the Mt. Shasta region, N California. Contrib Mineral Petrol 142:375–396
Grove T, Till C, Krawczynski M (2012) The role of H2O in subduction zone magmatism. Annu Rev Earth Planet Sci 40:413–439
Harris N, Pearce J, Tindle A (1986) Geochemical characteristics of collision-zone magmatism. In: Coward M, Ries A (eds) Collision tectonics. Geological Society Special Publication n°9, Blackwell Scientific Publications, London, pp 67–81
Harrison TM, Watson EB (1984) The behavior of apatite during crustal anatexis: equilibrium and kinetic considerations. Geochim Cosmochim Acta 48:1467–1477
Horn I, Foley S, Jackson S, Jenner G (1994) Experimentally determined partitioning of high field strength- and selected transition elements between spinel and basaltic melt. Chem Geol 117:193–218
Ionescu C (1997) Studiul metalogenetic al masivelor banatitice Budureasa şi Pietroasa (Munţii Bihor). PhD Thesis, Babeş–Bolyai, Cluj Napoca
Irvine T, Baragar W (1971) A guide to chemical classification of common volcanic rocks. Can J Earth Sci 8:315–341
Istrate G (1978) Petrological study of the Vlădeasa Massif (western part). Anu Inst Geol Geofiz 53:1–297
Jacobsen S, Wasserburg GJ (1980) Sm–Nd isotopic evolution of chondrites. Earth Planet Sci Lett 50:139–155
Johnson MC, Rutherford MJ (1989) Experimental calibration of the aluminium in hornblende geobarometer with application to Long Valley caldera (California) volcanic rocks. Geology 17:837–841
Joron JL, Bougault H, Wood D, Treuil M (1978) Application de la géochimie des éléments en traces à l'étude des propriétés et des processus de genèse de la croûte océanique et du manteau supérieur. Bull Soc Géol Fr XX(4):521–531
Kagami H, Ulmer P, Hansmann W, Dietrich V, Steiger R (1991) Nd–Sr isotopic and geochemical characteristics of the southern Adamello (northern Italy) intrusives: implications for crustal versus mantle origin. J Geophys Res 96:14331–14346
Klötzli U, Buda G, Skiöld T (2004) Zircon typology, geochronology and whole rock Sr–Nd isotope systematics of the Mecsek Mountain granitoids in the Tisia Terrane (Hungary). Mineral Petrol 81:113–134
Kohut M, Stein H, Uher P, Zimmermann A, Hraško L (2013) Re–Os and U–Th–Pb dating of the Rochovce granite and its mineralization (Western Carpathians, Slovakia). Geol Carpath 64:71–79
Kolb M, Von Quadt A, Peytcheva I, Heinrich CA, Fowler SJ, Cvetkovic V (2013) Adakite-like and normal arc magmas: distinct fractionation paths in the East Serbian segment of the Balkan–Carpathian arc. J Petrol 54(3):421–451
Kounov A, Schmid S (2013) Fission-track constraints on the thermal and tectonic evolution of the Apuseni mountains (Romania). Int J Earth Sci 102:207–233

Le Maitre RW (1989) A classification of igneous rocks and glossary of terms. Blackwell Scientific Publications, Oxford, p 193

Leake B, Woolley AR, Birch WD, Burke EAJ, Ferraris G, Grice JD, Hawthorne FC, Kisch HJ, Krivovichev VG, Schumacher JC, Stephenson NCN, Whittaker EJW (2004) Nomenclature of amphiboles: additions and revisions to the International Mineralogical Association's amphibole nomenclature. Mineral Mag 68(1):209–215

Liégeois JP, Navez J, Hertogen J, Black R (1998) Contrasting origin of post-collisional high-K calc-alkaline and shoshonitic versus alkaline and peralkaline granitoids. The use of sliding normalization. Lithos 45:1–28

Luhr J, Carmicahel I (1980) The Colima volcanic complex, Mexico. I: post-caldera andesites from Volcan Colima. Contrib Mineral Petrol 71:343–372

Macera P, Ferrara G, Pescia A, Callegari E (1983) A geochemical study on the acid and basic rocks of the Adamello batholith. Mem Soc Geol Ital 26:223–259

Martin H (1987) Petrogenesis of Archean trondhjemites, tonalites, and granodiorites from Eastern Finland: major and trace element geochemistry. J Petrol 28(5):921–953

McKay G (1989) Partitioning of rare earth elements between major silicate minerals and basaltic melts. In: Lipin, B, McKay, G. (eds), Geochemistry and mineralogy of REE. Mineralogical Society of America, Reviews in mineralogy, pp 45–77

Miyashiro A (1978) Nature of alkalic volcanic rock series. Contrib Mineral Petrol 66:91–104

Morimoto N (1989) Nomenclature of pyroxenes. Can Mineral 27:143–156

Müntener O, Kelemen P, Grove T (2001) The role of H2O during crystallization of primitive arc magmas under uppermost mantle conditions and genesis of igneous pyroxenites: an experimental study. Contrib Mineral Petrol 141:643–658

Nagasawa H (1973) Rare earth distribution in alkali rocks from Oki-Dogo Island, Japan. Contrib Mineral Petrol 39:301–308

Nagasawa H, Schnetzler C (1971) Partitioning of rare Earth, alkali, and alkaline Earth elements between phenocrysts and acidic igneous magmas. Geochim Cosmochim Acta 35:953–968

Nakamura Y, Fujimaki H, Nakamura N, Tatsumoto M (1986) Hf, Zr, and REE partition coefficients between ilmenite and liquid: implications for lunar petrogenesis. In: Proceedings of the 16th lunar and planetary science conference, pp D239–D250

Neubauer F (2002) Contrasting Late Cretaceous with Neogene ore provinces in the Alpine–Balkan–Carpathians–Dinaride collision belt. In: Blundell D, Neubauer F, von Quadt A (eds) The timing and location of major ore deposits in an evolving orogen. Geological Society of London, London, pp 90–100

Nicolae I, Seghedi I, Boboş I, do Rosarrio Azevedo M (2014) Permian volcanic rocks from the Apuseni Mountains (Romania): geochemistry and tectonic constraints. Chem Erde 74:125–137

Nicolescu S, Cornell D, Bojar A (1999) Age and tectonic setting of Bocşa and Ocna de Fier-Dognecea granodiorites (southwest Romania) and of associated skarn mineralisation. Miner Depos 34:743–753

Pană D, Heaman L, Creaser R, Erdmer P (2002) Pre-Alpine crust in the Apuseni Mountains, Romania: insights from Sm–Nd and U–Pb data. J Geol 110:341–354

Panaiotu C (1998) Paleomagnetic constraints on the geodynamic history of Romania. In: Sledzinski J, Ioane D (eds) Monograph of Southern Carpathians. Institute of Geodesy and Geodetic Astronomy, Warsaw University, pp 205–216

Pavelescu L, Pop G, Weisz E, Popescu G (1985) La nature et l'âgee du batholite banatitique de Bihor. In: XIII-th congress of KBGA, Cracow, Poland

Pearce J (1983) Role of the sub-continental lithosphere in magma genesis at active continental margins. In: Hawkesworth C, Norry M (eds) Continental basalts and mantle xenoliths. Shiva, Nantwich, pp 230–249

Pearce J, Peate D (1995) Tectonic implications of the composition of volcanic arc magmas. Annu Rev Earth Planet Sci 23:251–285

Pearce J, Harris N, Tindle A (1984) Trace element discrimination diagrams for the tectonic interpretation of granitic rocks. J Petrol 25(4):956–983

Peccerillo A, Martinotti G (2006) The western mediterranean lamproitic magmatism: origin and geodynamic significance. Terra Nova 18(2):109–117

Peccerillo A, Taylor SR (1976) Geochemistry of Eocene calc-alkaline volcanic rocks from the Kastamonu area, Northern Turkey. Contrib Mineral Petrol 58:63–81

Philpotts J, Schnetzler C (1970) Phenocryst-matrix partition coefficients for K, Rb, Sr and Ba, with applications to anorthosite and basalt genesis. Geochim Cosmochim Acta 34(3):307–322

Pin C, Santos Zalduegui JF (1997) Sequential separation of light rare-earth elements, thorium and uranium by miniaturized extraction chromatography: application to isotopic analyses of silicate rocks. Anal Chim Acta 339:79–89

Pin C, Briot D, Bassin C, Poitrasson F (1994) Concomitant separation of strontium and samarium-neodymium for isotopic analysis in silicate samples, based on specific extraction chromatography. Anal Chim Acta 298:209–217

Plank T, Langmuir C (1993) Tracing trace elements from sediment input to volcanic output at subduction zones. Nature 362:739–743

Popov P (1981) Magmatectonic features of the Banat-Srednogorie Belt. Geol Balc 11:42–73

Popov P, Berza T, Grubic A, Ioane D (2002) Late Cretaceous Apuseni–Banat–Timok–Srednogorie (ABTS) Magmatic and Metallogenic belt in the Carpathian–Balkan orogen. Geol Balc 32(2–4):145–164

Rădulescu D, Săndulescu M (1973) The plate-tectonics concept and the geological structure of the Carpathians. Tectonophysics 16:155–161

Rudnick R, Gao S (2003) The Composition of the continental crust. In: Rudnick RL (ed) The Crust, vol 3. In: Holland HD, Turekian KK (eds) Treatise on Geochemistry. Elsevier-Pergamon, Oxford, pp 1–64

Savu H (1996) Genesis and structure of the Mureş zone. Anu Inst Geol Rom 69:179–180

Schmid S, Bernoulli D, Fügenschuh B, Matenco L, Schefer S, Schuster R, Tischler M, Ustaszewski K (2008) The Alpine–Carpathian–Dinaridic orogenic system: correlation and evolution of tectonic units. Swiss J Geosci 101:139–183

Schuller V (2004) Evolution and geodynamic significance of the Upper Cretaceous Gosau basin in the Apuseni Mountains (Romania), Tübingen, 112 pp

Schuller V, Frisch W, Danišik M, Dunkl I, Melinte M (2009) Upper Cretaceous Gosau deposits of the Apuseni Mountains (Romania)—similarities and differences to the Eastern Alps. Austrian J Earth Sci 102:133–145

Sisson T (1994) Hornblende-melt trace element partitioning measured by ion microprobe. Chem Geol 117(1–4):331–344

Stefan A (1980) Petrographic study of the eastern part of the Vladeasa eruptive massif. Annu Inst Geol Geofiz 55:208–325

Stefan A, Lazar C, Intorsureanu I, Horvath A, Gheorghita I, Bratosin I, Serbanescu A, Calinescu E (1982) Petrological study of the banatitic eruptive rocks in the eastern part of the Gilau Mountains. D.S. Inst Geol Geofiz 69(1):215–246

Stefan A, Rosu E, Andar A, Robu L, Robu N, Bratosin I, Grabari G, Stoian M, Vajdea E (1992) Petrological and geochemical features of banatitic magmatites in northern Apuseni Mountains. Rom J Petrol 75:97–115

Steiger R, Jäger E (1977) Subcommission on geochronology: convention on the use of decay constants in geo- and cosmochronology. Earth Planet Sci Lett 36:359–362

Sun S, McDonough W (1989) Chemical and isotopic systematics of oceanic basalts: implications for mantle composition and processes. In: Saunders A, Norry M (eds) Magmatism in the ocean basins., Geological Society Special PublicationBlackwell Scientific Publications, Oxford, pp 313–345

Toplis M, Corgne A (2002) An experimental study of element partitioning between magnetite, clinopyroxene and iron-bearing silicate liquids with particular emphasis on vanadium. Contrib Mineral Petrol 144:22–37

Ulmer P, Callegari E, Sonderegger U (1983) Genesis of the mafic and ultramafic rocks and their genetical relations to the tonalitic-trondhjemitic granitoids of the southern part of the Adamello batholith (Northern Italy). Mem Soc Geol Ital 26:171–222

Vander Auwera J, Bologne G, Roelandts I, Duchesne JC (1998) Inductively coupled plasma-mass spectrometry (ICP-MS) analysis of silicate rocks and minerals. Geol Belgi 1(1):49–53

Venturelli G, Thorpe R, Dal Piaz G, Del Moro A, Potts P (1984) Petrogenesis of calc-alkaline, shoshonitic and associated ultrapotassic Oligocene volcanic rocks from the Northwestern Alps, Italy. Contrib Mineral Petrol 86:209–220

Villemant B (1988) Trace element evolution in the Phlegrean fields (central Italy)—fractional crystallization and selective enrichment. Contrib Mineral Petrol 98(2):169–183

von Blanckenburg F, Früh-Green G, Diethelm K, Stille P (1992) Nd-, Sr-, O-isotopic and chemical evidence for a two-stage contamination history of mantle magma in the Central-Alpine Bergell intrusion. Contrib Mineral Petrol 110:33–45

von Blanckenburg F, Kagami H, Deutsch A (1998) The origin of Alpine plutons along the Periadriatic Lineament. Schweiz Mineral Petrogr Mitt 78(1):55–66

Von Cotta B (1864) Erzlagerstätten im Banat und in Serbien. Braumüller, Wien, 108 pp

Von Quadt A, Moritz R, Peytcheva I, Heinrich C (2005) Geochronology and geodynamics of Late Cretaceous magmatism and Cu–Au mineralization in the Panagyurishte region of the Apuseni–Banat–Timok–Srednogorie belt, Bulgaria. Ore Geol Rev 27:95–126

Watson EB, Harrison TM (1983) Zircon saturation revisited: temperature and compositional effects in a variety of crustal magma types. Earth Planet Sci Lett 64:295–304

Wiesinger M, Neubauer F, Peytcheva I, von Quadt A, Berza T (2007) Geochemical characteristics of Surduc pluton (Upper Cretaceous), Romania: significance for banatite magmatism. In: Andrew C (ed) Digging deeper. Proceedings of the ninth biennial SGA meeting, Dublin, Ireland pp 913–916

Willingshofer E, Neubauer F, Cloetingh S (1999) The significance of Gosau-type basins for the Late Cretaceous tectonic history of the Alpine-carpathian belt. Phys Chem Earth (A) 24(8):687–695

Zimmerman A, Stein HJ, Hannah JL, Koželj D, Bogdanov K, Berza T (2008) Tectonic configuration of the Apuseni–Banat–Timok–Srednogorie belt, Balkans-South Carpathians, constrained by high precisions Re–Os molybdenite ages. Miner Deposita 43:1–21